GEOSPHERE

GEOSPHERE; v. 14, no. 2,

doi:10.1130/GES01537.1

14 figures; 1 table; 1 supplemental file

CORRESPONDENCE: igrevemeyer@geomar.de

CITATION: Grevemeyer, I., Ranero, C.R., and Ivandic, M., 2018, Structure of oceanic crust and serpentinization at subduction trenches: Geosphere, v. 14, no. 2, p. 395–418, doi:10.1130/GES01537.1.

Science Editor: Shanaka de Silva
Guest Associate Editor: Robert Stern

Received 27 March 2017
Revision received 25 August 2017
Accepted 8 December 2017
Published online 12 January 2018

Structure of oceanic crust and serpentinization at subduction trenches

Ingo Grevemeyer[1], Cesar R. Ranero[2,3], and Monika Ivandic[4]

[1]GEOMAR Helmholtz Centre for Ocean Research, Wischhofstrasse 1-3, Kiel 24148, Germany
[2]Instituto de Ciencias del Mar, CSIC, Pg. Marítim de la Barceloneta 37-49, Barcelona 08003, Spain
[3]ICREA, Pg. Lluís Companys 23, Barcelona 08010, Spain
[4]Department of Earth Sciences, Uppsala University, Villavägen 16, Uppsala 75236, Sweden

ABSTRACT

The subducting oceanic lithosphere may carry a large amount of chemically bound water into the deep Earth interior, returning water to the mantle, facilitating melting, and hence keeping the mantle mobile and, in turn, nurturing plate tectonics. Bending-related faulting in the trench–outer rise region prior to subduction has been recognized to be an important process, promoting the return flux of water into the mantle. Extensional faults in the trench–outer rise are opening pathways into the lithosphere, supporting hydration of the lithosphere, including alteration of dry peridotite to water-rich serpentine. In this paper, we review and summarize recent work suggesting that bend faulting is indeed a key process in the global water cycle, albeit not yet well understood. Two features are found in a worldwide compilation of tomographic velocity models derived from wide-angle seismic data, indicating that oceanic lithosphere is strongly modified when approaching a deep-sea trench: (1) seismic velocities in both the lower crust and upper mantle are significantly reduced compared to the structure found in the vicinity of mid-ocean ridges and in mature crust away from subduction zones; and (2) profiles shot perpendicular to the trench show both crustal and upper mantle velocities decreasing systematically approaching the trench axis, highlighting an evolutionary process because velocity reduction is related to deformation, alteration, and hydration. P-wave velocity anomalies suggest that mantle serpentinization at trenches is a global feature of all subducting oceanic plates older than 10–15 Ma. Yet, the degree of serpentinization in the uppermost mantle is not firmly established, but may range from <4% to as much as 20%, assuming that velocity reduction is solely due to hydration. A case study from the Nicaraguan trench argues that the ratio between P-wave and S-wave velocity (Vp/Vs) is a key parameter in addressing the amount of hydration. In the crust, the Vp/Vs ratio increases from <1.8 away from the trench to >1.9 in the trench, supporting the development of water-filled cracks where bend faulting occurs. In the mantle, the Vp/Vs ratio increases from ~1.75 in the outer rise to values of >1.8 at the trench, indicating the increasing intensity of serpentinization.

INTRODUCTION

At subduction trenches, two tectonic plates meet, and the denser incoming oceanic plate is forced down into the mantle, while the more buoyant continental or island-arc crust overrides the oceanic plate. This process of subduction facilitates a major flux of volatiles, including CO_2 and H_2O, into the deep subduction zone (e.g., Rüpke et al., 2009; Faccenda et al., 2009; van Keken et al., 2011; Freundt et al., 2014), controlling slab melting (Rüpke et al., 2004) and intermediate-depth seismicity of Wadati-Benioff zones (Green and Houston, 1995). It has been long considered that most water trapped in the subducting plate would reside in the top of the subducting oceanic plate, called the upper oceanic crust, formed by extrusive lavas and sheeted dikes where large-scale porosity and high permeability nurtures hydrothermal circulation. In contrast, the low permeability of the lower crust suggests that the gabbroic lower crust and the peridotitic upper mantle below would remain considerably dry (e.g., Wallmann, 2001; Jarrard, 2003).

Alteration, however, is driven by the fluid-rock ratio, and hence a number of processes may facilitate hydration of the oceanic lithosphere during its life cycle. On- and off-axis hydrothermal circulations (Stein and Stein, 1994) are perhaps the best-studied processes changing the properties of the oceanic lithosphere (Alt et al., 1986, 1996). Further, crustal formation itself affects the structure and composition of the crust. Key factors affecting crustal formation include spreading rate (White et al., 2001) and mantle temperature (Klein and Langmuir, 1987; McKenzie and Bickle, 1988; Korenaga et al., 2002), resulting in compositional variations and crustal thickness variations from <3 km (White et al., 2001) to >10 km when crust is formed in the vicinity of hotspots (Hopper et al., 2003; White et al., 2008). Crust formed at slow to ultra-slow spreading rates may also suffer from tectonism and core-complex formation (e.g., Cann et al., 1997; Dannowski et al., 2010; Reston and Ranero, 2011), unroofing lower crust and upper mantle to the seafloor and hence causing alteration and hydration. After crustal formation at a spreading center, alteration is generally confined to the uppermost permeable crust and decays with time.

During alteration, the basaltic rocks take up H_2O, forming phillipsite, smectite, and Fe-Mn oxides (Alt et al., 1986, 1996). Geochemical alteration proceeds inward, particularly along cracks and veins. Secondary minerals formed during weathering of the rocks are smectites, celadonite, analcite, and carbonates. Thus, they increase the amount of bound water in the upper crust and are an important source of bound water within the subducting oceanic plate. Over millions of years, off-axis hydrothermal mineralization fills cracks, fissures, and veins. Thereby, initial porosity of 14%–17% estimated to occur in juvenile uppermost crust at ridge crests is reduced to 4%–8% in mature uppermost crust (Gillis and Sapp, 1997); in turn, seismic velocity of the uppermost igneous basement increases with age from values of ~2.5 km/s at ridge crests to 4.5 km/s in mature oceanic crust (Grevemeyer and Weigel, 1996, 1997; Carlson, 1998). With time, hydrothermal circulation shuts off when impermeable sediment blankets the igneous crust and restricts the flow of seawater into the basement. However, when the subducting plate approaches a deep-sea trench, outer-rise faulting (Ranero et al., 2003; Grevemeyer et al., 2005, 2007) may create pathways into the lithosphere, facilitating volatile fluxes into the uppermost mantle lithosphere.

Thus, at trenches, a growing body of observational evidence collected during the last ~10 years suggests that the incoming oceanic lithosphere is modified in the outer-rise area seaward of the trench axis (Ranero et al., 2003; Peacock, 2004; Grevemeyer et al., 2007; Fujie et al., 2013). The outer rise is a consequence of the flexure of the subducting lithosphere, producing a prominent bathymetric bulge seaward of the trench axis (Bodine and Watts, 1979; Levitt and Sandwell, 1995; Hunter and Watts, 2016). Although uplift starts several hundreds of kilometers from the trench, bending is strongest within 50 km of the trench axis. Seafloor mapping (Masson, 1991; Ranero et al., 2005; Hunter and Watts, 2016) and earthquake distributions and focal mechanisms in this area (Chapple and Forsyth, 1979; Lefeldt and Grevemeyer, 2008; Emry and Wiens, 2015) are consistent with bending-related normal faulting. These faults, called bend faults, are suggested to provide the pathways for fluids to enter the crust and mantle (Ranero et al., 2003). In areas with little sediment cover upon the incoming plate, like Chile and Nicaragua, heat-flow anomalies (Grevemeyer et al., 2005) suggest that hydrothermal circulation is more vigorous where bend faults breach the seafloor and thus may govern fluid flow into the crust. Electromagnetic data collected across the outer rise offshore of Nicaragua illuminate the infiltration of seawater along bend faults (Naif et al., 2015). Lastly, seismic reflection imaging of the incoming oceanic lithosphere detected faults cutting through the entire crust into the uppermost mantle (Ranero et al., 2003). The strong reflectivity of the faults may suggest that seawater indeed migrates along the faults down to mantle depth, altering dry peridotites to hydrous serpentine.

Wide-angle seismic surveys of the incoming oceanic plate seaward of deep-sea trenches suggest that seismic velocities in both crust and mantle are significantly lower than in mature oceanic lithosphere (e.g., Ranero and Sallarès, 2004; Grevemeyer et al., 2007; Contreras-Reyes et al., 2011; van Avendonk et al., 2011). Those conclusions are drawn from the interpretation that the structure at trenches deviates from "typical" oceanic crust (e.g., White et al., 1992). The reference structure of the oceanic crust is generally based on the compilation of wide-angle seismic data by White et al. (1992) collected more than 25 years ago, when the number of available ocean-bottom seismometers (OBSs) was small and hence the spacing of seismic receivers along profiles was in the order of several tens of kilometers. In consequence, data analysis differed from modern state-of-the-art inversion techniques (e.g., van Avendonk et al., 1998; Korenaga et al., 2000) and is therefore not appropriate to provide the reference for modern tomographic studies. For example, the classical compilation of White et al. (1992) used waveform modeling of single shot gathers to yield one-dimensional (1-D) velocity-depth profiles and crustal thickness. Today, wide-angle seismic surveys use densely spaced OBS stations and either detailed forward modeling utilizing ray tracing (Zelt and Smith, 1992) or inversion with joint refraction and reflection tomography (e.g., van Avendonk et al., 1998; Korenaga et al., 2000). Therefore, changes in available data quality and modeling methods argue for revisiting the structure of the oceanic crust, providing a new reference for the seismic velocity structure derived from seismic tomography. We will particularly focus on the structure of the Pacific Basin, where most subduction zones occur. Further, we will review velocity changes of crust and upper mantle in the vicinity of trenches, yielding insights into the degree of hydration of the subducting lithosphere and surveying how bend faulting affects the seismic properties of the lithosphere, including serpentinization.

GLOBAL COMPILATIONS

Since the late 1940s, exploration of the deep sea and the sub-seafloor structure has changed our view of the ocean basins dramatically, eventually resulting in the concept of plate tectonics. One key feature was the observations that the thickness and seismic structure of the oceanic crust are very much different from those of the continental crust (e.g., Raitt, 1963). Since the early days of academic ocean-floor exploration, both technology and inversion procedures have changed, affecting our views on what the oceanic crust looks like. Here, we briefly review the current state-of-the-art reference model, based on the global compilation of White et al. (1992). In addition, we review the structure derived by White et al. (1992) in light of new data acquired over the past 30 years.

Thickness of Oceanic Crust, A.D. 1992

The primary source of our knowledge of the structure of the entire oceanic crust is the interpretation of seismic refraction experiments. The first classic compilation of seismic data of Raitt (1963) was based on the traditional slope-intercept method. Thus, seismic profiles were interpreted using straight-line least-squares fits to the first arrivals, inverting them to a layered

Grevemeyer et al.; GEOSPHERE - Supplementary Table 1:

Lon	Lat	Age	rate	thickness	error	Area	Reference
40.0	86.4	0	6	2.7	1.5	Gakkel	Jokat and Schmidt-Ausch, 2007
41.0	86.4	0	6	2.7	1.5	Gakkel	Jokat and Schmidt-Ausch, 2007
45.0	86.6	0	6	2.6	1.5	Gakkel	Jokat and Schmidt-Ausch, 2007
46.0	86.7	0	6	2.7	1.5	Gakkel	Jokat and Schmidt-Ausch, 2007
50.0	86.8	0	6	3.3	1.5	Gakkel	Jokat and Schmidt-Ausch, 2007
54.0	87.0	0	6	2.9	1.5	Gakkel	Jokat and Schmidt-Ausch, 2007
62.0	86.9	0	6	3.5	1.5	Gakkel	Jokat and Schmidt-Ausch, 2007
16.0	85.5	0	10	2.5	1.5	Gakkel	Jokat and Schmidt-Ausch, 2007
12.0	84.9	0	10	1.4	1.5	Gakkel	Jokat and Schmidt-Ausch, 2007
35.0	85.8	0	10	1.9	1.5	Gakkel	Jokat and Schmidt-Ausch, 2007
38.0	86.0	0	10	2.1	1.5	Gakkel	Jokat and Schmidt-Ausch, 2007
6.0	84.5	0	13	3.2	1.5	Gakkel	Jokat and Schmidt-Ausch, 2007
5.1	83.8	0	13	1.2	1.2	Gakkel	Jokat and Schmidt-Ausch, 2007
5.0	83.8	0	13	4.9	1.5	Gakkel	Jokat and Schmidt-Ausch, 2007
-3.0	83.6	0	13	2.5	1.5	Gakkel	Jokat and Schmidt-Ausch, 2007
65.8	-27.7	2	12	4.5	0.8	SWIR 66°E	Muller et al., 1999
66.2	-27.7	2	12	3.2	0.8	SWIR 66°E	Muller et al., 1999
57.0	-32.7	11	14	3.8	1.0	SWIR 57°E	Muller et al., 2000
3.0	72.4	5	15.5	4.1	0.5	Mohns	Klingelhoefer et al., 2000
-12.2	-4.8	<15	32	5.5	0.5	MAR 5°S	Planert et al., 2009
-12.2	-4.8	<15	32	3.0	0.5	MAR 5°S	Planert et al., 2009
-12.2	-4.8	<15	32	9.0	0.2	MAR 5°S	Planert et al., 2009
-12.2	-4.8	<15	32	6.0	0.8	MAR 5°S	Planert et al., 2009
-11.5	-5.2	<15	32	4.0	0.8	MAR 5°S	Planert et al., 2010
-11.5	-5.2	<15	32	3.0	0.5	MAR 5°S	Planert et al., 2010
-11.5	-5.2	<15	32	4.5	0.7	MAR 5°S	Planert et al., 2010
-11.5	-5.2	<15	32	3.5	0.7	MAR 5°S	Planert et al., 2010
-11.5	-5.2	<15	32	3.6	0.5	MAR 5°S	Planert et al., 2010
-11.5	-5.2	<15	32	2.6	0.5	MAR 5°S	Planert et al., 2010
-11.5	-5.2	<15	32	2.5	0.4	MAR 5°S	Planert et al., 2010
-45.0	23.3	<12	25	2.4	0.8	MAR 23°N	Canales et al., 2000
-44.8	23.3	<12	25	4.5	0.8	MAR 23°N	Canales et al., 2000
-36.4	35.0	0	22	8.1	0.5	MAR 35°N	Hooft et al., 2000
-37.2	34.4	0	22	9	0.5	MAR 35°N	Hooft et al., 2000
-37.8	33.8	0	22	6.6	0.5	MAR 35°N	Hooft et al., 2000
-37.8	33.6	0	22	2.5	0.5	MAR 35°N	Hooft et al., 2000
-37.2	34.8	0	22	5.0	0.5	MAR 35°N	Hooft et al., 2000
-36.2	35.1	0	22	3.5	0.5	MAR 35°N	Hooft et al., 2000
-44.9	22.3	<10	26	8.0	0.5	MAR 22°N	Dannowski et al., 2010
-45.2	22.3	<10	26	4.0	0.5	MAR 22°N	Dannowski et al., 2010
-45.4	22.3	<10	26	6.0	0.5	MAR 22°N	Dannowski et al., 2010
-45.3	21.7	0	26	3.8	0.5	MAR 21°N	Dannowski et al., 2011
-45.3	21.3	0	26	7.8	0.5	MAR 21°N	Dannowski et al., 2011
-45.4	21.5	0	26	5.0	0.5	MAR 21°N	Dannowski et al., 2011
-45.2	22.0	<10	26	6.5	0.5	MAR 21°N	Dannowski et al., 2011
49.5	-37.6	0	14	5.5	0.5	SWIR 50°E	Nui et al., 2015
50.5	-37.6	0	14	9.5	0.5	SWIR 50°E	Nui et al., 2015

[1]Supplemental Tables. Table S1: Details on seismic surveys providing crustal thickness estimates supplementing the compilation of van Avendonk et al. (2017) shown in Figures 1A and 2. Table S2: Details on seismic surveys providing crustal thickness and lower crustal velocity estimates shown in Figure 1B and Figure 3. Table S3: Field of the magmatic crust ensemble from velocity depth functions from 2-D seismic surveys shown in Figures 4, 5, and 7. Table S4: Field of Pacific crust ensemble from velocity depth functions from 2-D seismic surveys shown in Figures 6 and 8. Table S5: Fields of Atlantic crust ensembles from velocity depth functions from 2-D seismic surveys. (A) Spreading segment centers; (B) spreading segment end; and (C) combination of spreading segment centers and ends shown in Figure 7. Please visit http://doi.org/10.1130/GES01537.S1 or the full-text article on www.gsapubs.org to view the Supplemental Tables.

velocity-depth structure using the slopes and intercepts of the best-fitting lines. Raitt (1963) subdivided the crust into three distinct layers, which have formed the reference basis for seismic profiles ever since. The upper oceanic crust has been called "layer 2" and the lower crust "layer 3". In contrast to the interpretation of Raitt (1963), it was later shown that the upper igneous crust is a region of strong velocity gradients, while the lower crust is relatively homogeneous, although it does show an increase in velocity with depth (e.g., Whitmarsh, 1978; White et al., 1992). The lower crust, or layer 3, often called the "oceanic layer", is inferred to be composed of gabbros (e.g., White et al., 1992; Carlson and Miller, 2004). As crust ages, sediments accumulate on the igneous basement, creating "layer 1".

Raitt (1963) recognized that the oceanic crust is remarkably uniform. He showed that crust is 6.57 ± 1.61 km thick. Three decades later, Chen (1992) suggested that average oceanic crust is ~6 km thick, and White et al. (1992) estimated a thickness of 7.08 ± 0.78 km away from anomalous regions such as fracture zones and hotspots, with extremal bounds of 5.0–8.5 km. The large differences between the studies may arise from the fact that interpretation methods have changed over time. Indeed, it was found that the traditional slope-intercept solution used by Raitt (1963) considerably underestimates the depth to the Moho when compared to synthetic seismogram modeling (e.g., White et al., 1992) or other techniques that allowed the seismic velocity in oceanic crust to increase relatively smoothly with depth as a series of gradients rather than in two or three uniform velocity layers. However, a more recent compilation of seismic crustal thickness estimates (Figs. 1 and 2) showed that a large degree of variability remains (van Avendonk et al., 2017) and Table S1[1], suggesting that accretion of oceanic crust itself is highly variable in time and space.

A key factor controlling the variability of the oceanic crust might be mantle temperature (Klein and Langmuir, 1987; Dalton et al., 2014; Dick and Zhou, 2014). One of the best-documented features is that crust formed near hotspots is generally thicker than crust formed away from hotspots (e.g., White et al., 1992; Korenaga et al., 2002). Further, van Avendonk et al. (2017) argued that the upper mantle may have cooled by 15–20 °C per 100 m.y. on average since 170 Ma, suggesting that oceanic crust was 1.7 km thicker on average in the mid-Jurassic than crust produced along the present-day mid-ocean ridge system (Fig. 2A). Indeed, the oldest crust of the northwestern Pacific plate is in the order of 7.1–7.4 km thick (Reston et al., 1999; Oikawa et al., 2010), while young crust formed at the southern East Pacific Rise ranges in thickness from 5.1 km to 5.7 km at 16°S (Canales et al., 1998) and from 5.6 to 6.3 km at 14°S (Grevemeyer et al., 1998). Offshore of Nicaragua, crust of ca. 24 Ma age ranges from 4.8 to 5.5 km (Grevemeyer et al., 2007; Ivandic et al., 2008), and 9–18 Ma crust formed at the Chile Ridge averages 5.3 km (Contreras-Reyes et al., 2007). However, 30–40 Ma crust subducting in Chile between 20°S to 40°S is much thicker, ranging from 6 km to 8 km (Ranero and Sallarès, 2004; Contreras-Reyes et al., 2008; Moscoso and Grevemeyer, 2015), and even crust formed today at the northern East Pacific Rise at 8°N to 10°N varies from 6 to ~7.5 km (Canales et al., 2003), highlighting the fact that other processes rather than age alone may contribute to control the thickness of the crust.

Slow- and ultraslow-spreading ridges show an even larger variability of crustal thickness when compared to crust formed along intermediate- and fast-spreading ridges of the Pacific Ocean (Fig. 2B). At slow-spreading ridges, crustal thickness varies as a function of segmentation, supporting focused mantle upwelling at the center of segments (Lin and Phipps Morgan, 1992; Tolstoy et al., 1993). Thus, the thickest crust is found in the middle of spreading segments (7–9 km), while at the end of spreading segments, crust is much thinner (4–6 km) (e.g., Canales et al., 2000a; Hooft et al., 2000; Planert et al., 2009; Dannowski et al., 2011), displaying a large degree of thickness variations at slow spreading rates of 20–50 mm/yr (Fig. 2B). Ultraslow spreading rates of <20 mm/yr have been believed to mark an abrupt decrease in amount of melt generated at the spreading center (White et al., 2001). However, the paucity of data collected in the Arctic and at the Southwest Indian Ridge left the proposition speculative. Today, we know that even at ultraslow spreading rates, crustal thickness ranges from <3 km (Jackson et al., 1982; Jokat and Schmidt-Aursch, 2007) to >9 km (Niu et al., 2015; Li et al., 2015). Despite the strong variability in crustal thickness, ultraslow-spreading crust seems to be on average thinner than crust formed at higher spreading rates (Fig. 2B).

Seismic Velocity Structure of the Oceanic Crust, A.D. 1992

The formation process of the oceanic lithosphere at mid-ocean ridges is shaping the structure of the oceanic crust. The upper igneous crust, or layer 2, is ~1.5–2 km thick, with a region of strong velocity gradients with velocities increasing from ~3 km/s to ~6.7 km/s at its base. The seismic velocities in the extrusive lava pile or uppermost crust are typically only one-third to one-half of measured laboratory values of unfractured basalts (e.g., Hyndman and Drury, 1976; Grevemeyer and Bartetzko, 2004). This significant discrepancy has long been recognized and has been satisfactorily explained by the presence of large-scale porosity in the uppermost crust. Increase in velocity with depth results from a reduction of this large-scale porosity (e.g., Hyndman and Drury, 1976; Whitmarsh, 1978). The lower part of layer 2 is formed by the sheeted dike complex (Wilson et al., 2006). The boundary between layers 2 and 3 shows primarily a decrease in vertical velocity gradient from > 1 km/s per km to 0.1 km/s per km, with a velocity increase from ~6.7 km/s at the transition zone to ~7.0 km/s near the crust-mantle boundary (Carlson and Miller, 2004), suggesting that the physical properties of layer 3 are relatively homogeneous at seismic scale. Layer 3 includes more than two-thirds of the igneous crust (e.g., White et al., 1992). It is interesting to note that White et al. (1992) reported that velocity in layer 3 may reach values of up to 7.6 km/s. However, such high values are inconsistent with the idea that the layer is formed by gabbroic rocks (Carlson and Miller, 2004). Thus, extremal values reported for layer 3 by White et al. (1992) might be associated with a Moho transition zone, where gabbro

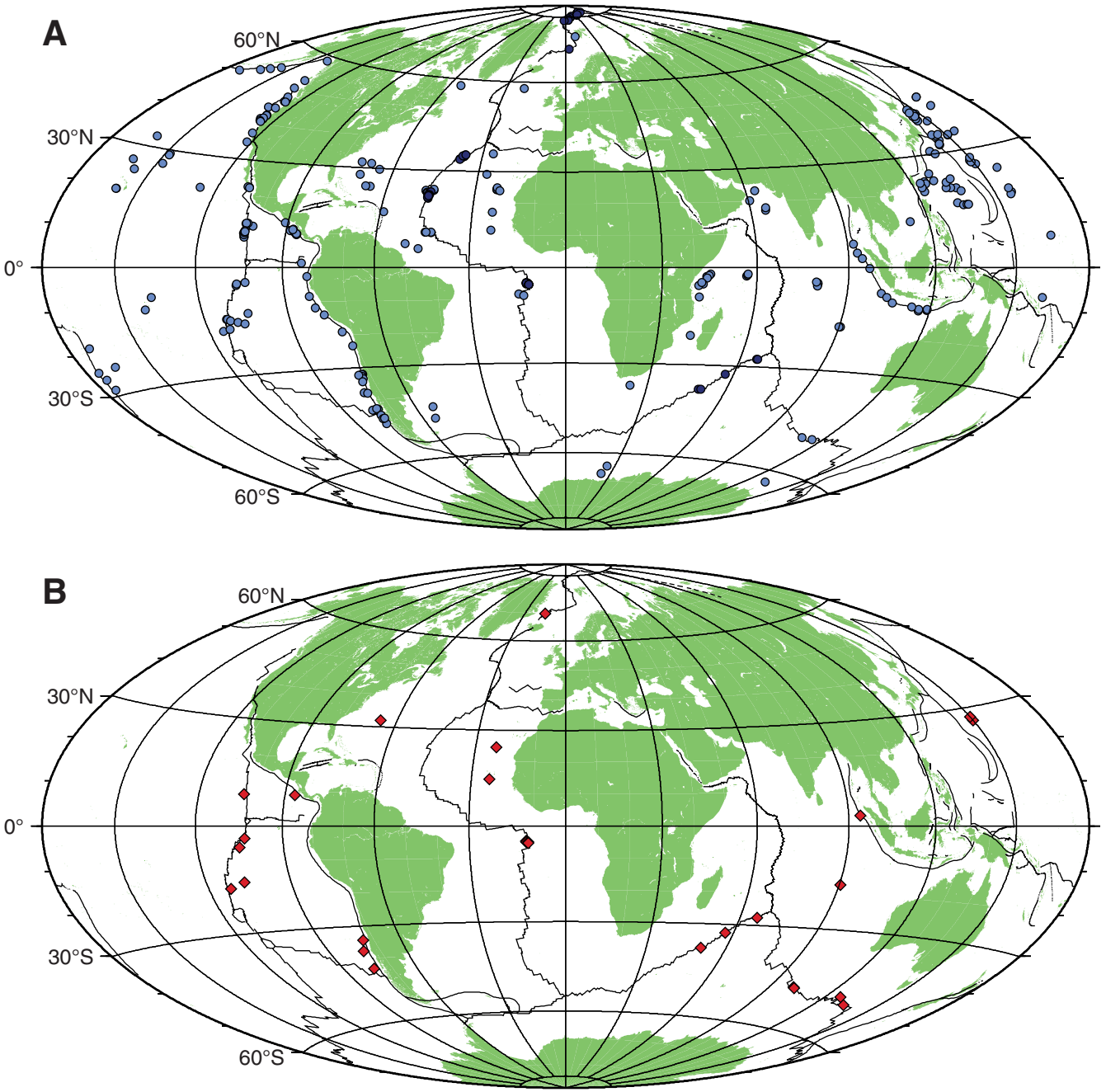

Figure 1. (A) Global map of seismic data providing oceanic crustal thickness (data sources: light blue dots, data compiled by van Avendonk et al. (2017); dark blue dots, data summarized in Table S1 [footnote 1]). Crustal thickness estimates are shown in Figure 2. (B) Global map of seismic data providing both crustal thickness and detailed errors on seismic velocity using modern state-of-the-art inversion techniques (data source: Table S2 [footnote 1]). Crustal thickness versus lower-crustal velocity is shown in Figure 3. Thin black lines indicate plate boundaries.

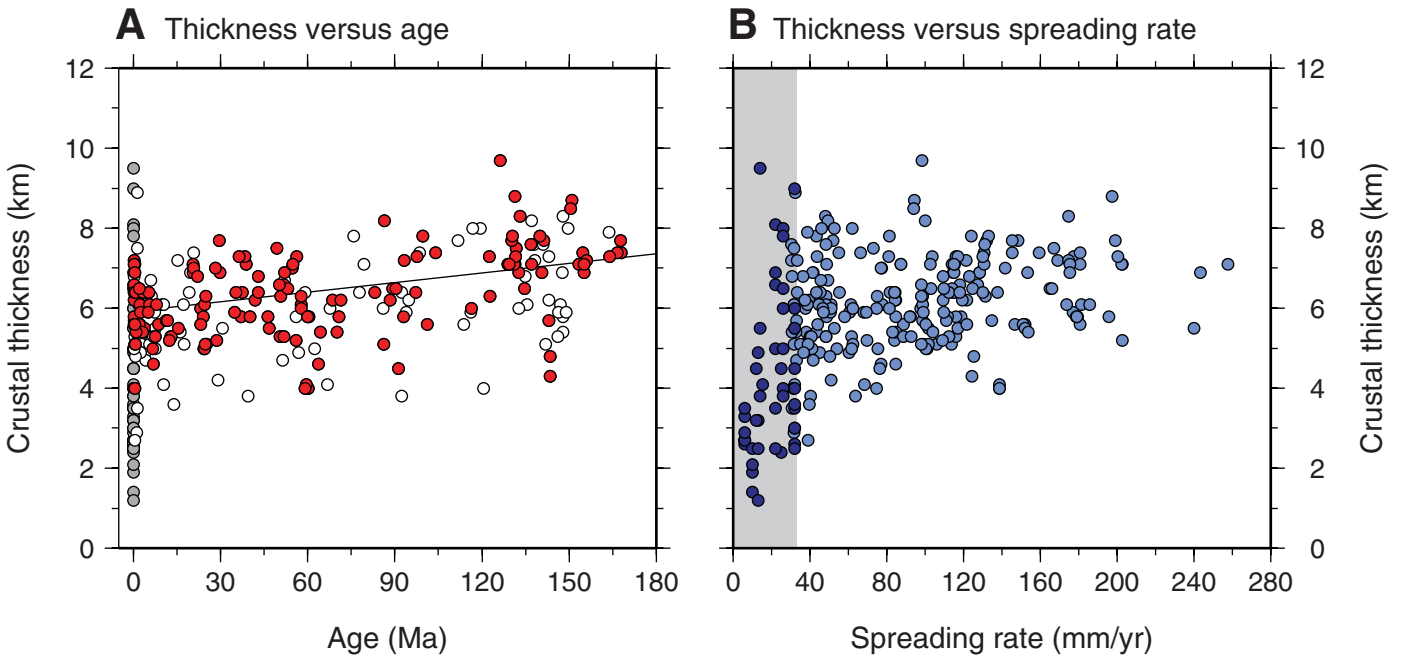

Figure 2. (A) Crustal thickness versus lithospheric age. Red and white dots are from van Avendonk et al. (2017) and represent thickness estimates from the Pacific and Atlantic-Indian Oceans, respectively; gray dots are additional estimates from either zero-age crust or from spreading rates <30 mm/yr not included in the van Avendonk et al. (2017) study. Black line indicates the trend of decreasing crustal thickness with time derived by van Avendonk et al. (2017) for the Pacific Basin. (B) Crustal thickness versus spreading rate. Light blue dots are estimates compiled by van Avendonk et al. (2017); dark blue dots are additional estimates from either zero-age crust or from spreading rates <30 mm/yr; gray area marks spreading rates <30 mm/yr. Additional data are in Table S1 (footnote 1). Worldwide distribution of surveys is shown in Figure 1A.

sills alternate with mantle dunites, as observed in some ophiolites (Karson et al., 1984), rather than being due to crustal rocks, or may even represent serpentinized mantle.

White et al. (1992) compiled velocity-depth profiles from both the Pacific Ocean and the Atlantic Ocean, which formed the reference for a wealth of seismic studies worldwide. However, as indicated in Figure 2, crustal thickness and hence formation conditions may vary both with spreading rate and age. Consequently, the compilation of White et al. (1992) averages a number of studies sampling crust formed at different spreading environments. Further, the 1-D nature of velocity estimates averages the information over tens of kilometers in horizontal distance (e.g., Minshull et al. 1991) and hence may cause a significant bias of the velocity-depth structure. It is therefore appropriate to estimate a reference model that considers modes of crustal accretion and uses only the most reliable data with a robust estimation of velocity uncertainties inherently related to seismic data inversion. Last, we like to define a reference model that allows us to reveal and study processes rather than classifying crust with respect to its geography.

A NEW REFERENCE MODEL FOR OCEANIC CRUST STRUCTURE

Data Selection

The porous upper oceanic crust is strongly affected by eruptive dynamics (e.g., Perfit and Chadwick, 1998). In contrast, the velocity structure of the lower oceanic crust formed at intermediate to fast spreading rates reflects the process of mantle melting at the spreading center. The amount of melt produced by adiabatic decompression of the mantle and the composition of the resultant igneous crust depend on the temperature, composition, and water content of the mantle source (e.g., Klein and Langmuir, 1987; McKenzie and Bickle, 1988; Korenaga et al., 2002; Sallarès et al., 2005). Normal oceanic crust with a thickness of ~6 km (e.g., Chen, 1992) and mid-ocean ridge basalt (MORB)–like composition is the result of decompressional melting of a mantle source composed of dry pyrolite with a mantle temperature of ~1300 °C (McKenzie and Bickle, 1988). Thus, crustal formation occurs as a passive response to seafloor spreading (i.e., passive upwelling). Higher mantle temperatures

or compositional anomalies may cause buoyant upwelling of the mantle (i.e., active upwelling). The combination of active upwelling and higher mantle temperatures, or the presence of a more fertile mantle source, will produce larger amounts of melting and, likely, a thicker crust. Crustal thickness and lower-crustal velocity have been used as proxies in surveying the effects of mantle melting on crustal accretion (e.g., Korenaga et al., 2002).

In Figure 3, we plot seismic estimates of lower-crustal velocity based on modern wide-angle seismic data with control on the error bounds. Our preferred type of data is from seismic travel-time tomography using jointly inverted first arrivals and wide-angle reflections, yielding both crustal thickness and velocity structure, and typically with estimated uncertainty. Data of Figure 3 are summarized in Table S2 (footnote 1). To increase the number of studies, we had to include some modern-experiment results obtained with forward modeling yielding data covering a wider range of spreading rates, including ultraslow and ultrafast spreading rates (Fig. 3). However, we assigned to estimates derived from forward modeling larger uncertainties compared to tomographic inversions, as forward modeling is accompanied by larger degrees of freedom in the modeling procedure and poorer misfit to the data.

In addition, it might be important to reject data acquired at juvenile seafloor. At the Mid-Atlantic Ridge, Purdy and Detrick (1986) noted that within the median valley, crustal structure may deviate from that of mature crust. They found a crustal structure with some characteristics of simple mature oceanic crust including a well-defined Moho transition zone. However, the velocity in layer 3 of ~6.5 km/s was lower than in mature crust off-axis. They concluded that on-axis hydrothermal circulation presents an evolutionary process that penetrates to the base of the crust, cooling the upper mantle and precipitating secondary minerals into crustal cracks and fissures, sufficient to lower the porosity and increase the velocity by several percent. Consequently, with time, the crack-filling process progressed upward though the crust, leaving behind a homogeneous low-gradient layer 3. This scenario is consistent with observations from the Southeast Indian Ridge, where Holmes et al. (2008) observed that profiles running along the ridge crest provided a lower velocity in layer 3 than in crust sampled off-axis. Away from the ridge crest, fast-spreading lower crust did not show any age-dependent features (Grevemeyer et al., 1998). We therefore tried to exclude zero-age data in our assessment. However, due to the fact that basically all data from ultraslow-spreading ridges were collected along the ridge crest, we relaxed

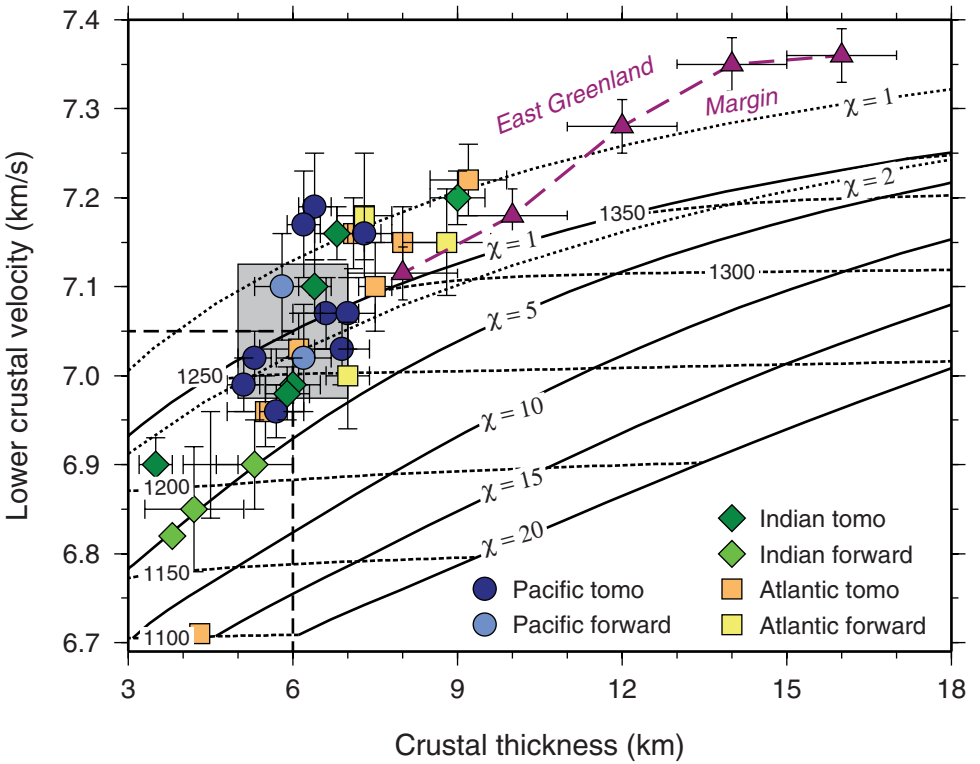

Figure 3. Crustal thickness versus lower-crustal velocity for the Pacific, Indian, and Atlantic Oceans from either tomography (tomo) or forward modeling, and detailed error analysis (Table S2 [footnote 1]), providing tight constraints on the physical properties of the crust (data are summarized in Table S2 [footnote 1]). Data from East Greenland are from Hopper et al. (2003). In addition, the figure shows two models relating mantle melting to upwelling (χ) and to mantle temperature (only shown for the Sallarès et al. [2005] model; thin broken lines with labeled temperatures of 1100–1350 °C): thick solid lines are from a two-dimensional melting model of Sallarès et al. (2005), and thick dotted lines are from a one-dimensional melting model of Korenaga et al. (2002). Gray area marks an area which varies by ±1 km in thickness and ±1% in velocity from a 6-km-thick crust (as defined by Sallarès et al. [2005], assuming passive upwelling) and a lower-crustal velocity of 7.05 km/s (values marked with thick dashed lines). Studies within the field represent our reference crust compiled in Figure 4. Worldwide distribution of surveys is shown in Figure 1B.

the criteria for ultraslow-spreading ridges for completeness, even though those velocities may be affected by local processes like deep hydrothermal activity. Table S2 [footnote 1] summarizes the data plotted in Figure 3.

Plotting lower-crustal velocity versus crustal thickness (Fig. 3) illustrates a striking relationship. Thicker crust has faster lower-crustal P-wave velocities than thinner crust. Korenaga et al. (2002) and Sallarès et al. (2005) provided a steady-state mantle melting model, including deep damp melting, that could be used to survey the relationship between mantle temperature, upwelling, and mantle composition on the one hand, and lower-crustal seismic velocity and crustal thickness on the other hand. A set of parameters is needed to define a reference model. Crustal thickness *H* and lower-crustal velocity Vp are calculated for mantle potential temperatures varying from 1100 to 1350 °C and an upwelling ratio (rising velocity over surface divergence) at the base of the damp melting zone, χ, varying from 1 to 20. Mantle temperature itself is still a matter of debate. Thus, with respect to the model of Sallarès et al. (2005), the melting model of Korenaga et al. (2002) provides temperatures ~50 °C higher (~1350 °C), and Dalton et al. (2014) found mantle temperatures below the global mid-ocean ridge system varying from ~1350 °C to 1450 °C. However, an assessment of mantle temperature is beyond of our scope, but the observation of crustal thickness increasing with increasing temperature is a robust and common feature.

Our compilation of seismic data indicates that the majority of seismic data from fast- and intermediate-spreading ridges result in a crustal thickness of 6 ± 1 km. For crust thicker than ~7 km and hence toward higher mantle temperatures, the theoretical predictions (χ = 1) roughly approximate the observed P-wave velocity versus crustal thickness trend. For crust thinner than ~5 km, however, the relationship breaks down, suggesting that crustal properties are affected by faulting and fracturing, which in turn reduces lower-crustal seismic velocities. Thin crust reported in Figure 3 generally occurs at segment ends of slow-spreading ridges (e.g., Canales et al., 2000a; Planert et al., 2009) or has been generated at ultraslow spreading rates (e.g., Minshull et al., 2006; Niu et al., 2015). Exceptions to the rule include data from the Australian-Antarctic discordance (Holmes et al., 2010).

To derive the reference model, we used all results from wide-angle seismic surveys conducted at intermediate- and fast-spreading ridges, providing a crustal thickness of 6 ± 1 km and an average lower-crustal velocity of 7.05 km/s ± 1%, which represents the structure formed by passive decompression (χ ~1) melting of a dry pyrolitic mantle (Fig. 3) (Sallarès et al., 2005). The ensemble was obtained from velocity-depth functions extracted from two-dimensional (2-D) velocity models (Fig. 4). We call it the "magmatic crust ensemble" (Table S3 [footnote 1]). All ensembles were derived in the same way. Thus, we used

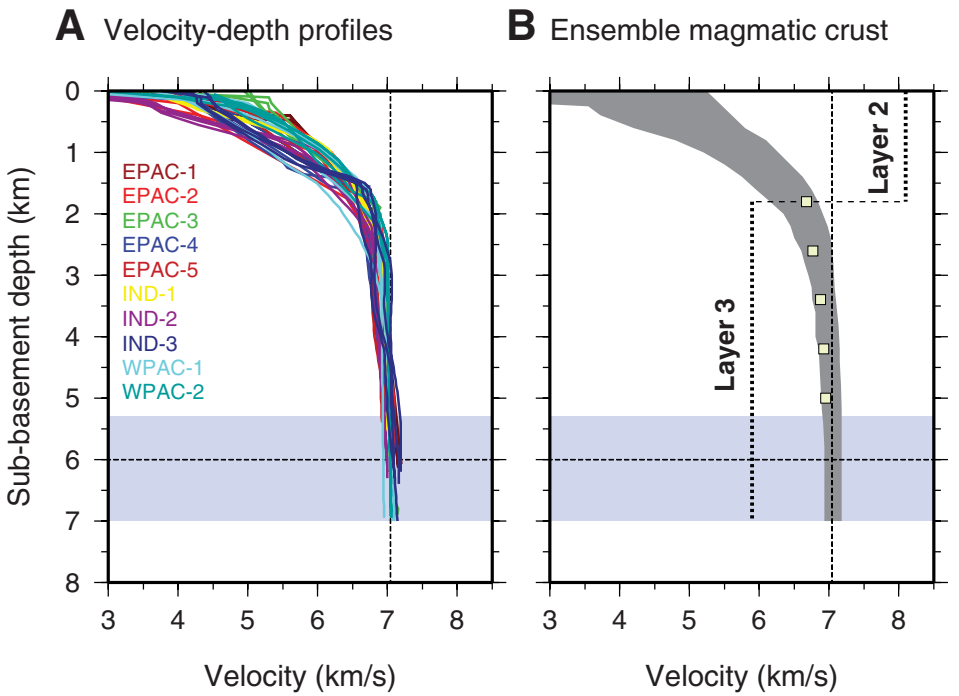

Figure 4. (A) Velocity-depth profiles of magmatic crust varying less than ±1 km in thickness and ±1% in velocity from a 6-km-thick crust with a lower-crustal velocity of 7.05 km/s (values marked with dashed lines). Profiles are derived from intermediate- and fast-spreading crust from the Pacific and Indian Oceans. Sources: EPAC-1—Grevemeyer et al. (1998); EPAC-2—Canales et al. (1998, 2003); EPAC-3—Contreras-Reyes et al. (2008); EPAC-4—Contreras-Reyes et al. (2007); EPAC-5—Moscoso et al. (2011); IND-1—line 2 of Holmes et al. (2008); IND-2—line 4 of Holmes et al. (2008); IND-3—stations in the Wharton Basin of Grevemeyer et al. (2001); WPAC-1—line MTr8 of Oikawa et al. (2010); WPAC-2—line MTr6 of Oikawa et al. (2010). (B) Ensemble derived from the velocity-depth profiles, providing our magmatic crust ensemble. Blue area marks variation in crustal thickness found in the velocity-depth profiles. Yellow squares are estimates of lower-crustal velocity from Carlson and Miller (2004) shifted by 1 km downward in depth. Depth range of basaltic layer 2 and gabbroic layer 3 are shown by labeled dotted lines. Dashed lines at 6 km depth and 7.05 km/s velocity indicate reference crustal thickness and reference lower crustal velocity as defined by passive upwelling using the model of Sallarès et al. (2005) (see Fig. 3).

2-D tomographic models and extracted every 10 km a 1-D velocity-depth profile, capturing the variability of the 2-D velocity model. If velocity-depth functions were derived from forward models (Canales et al., 1998; Grevemeyer et al., 1998), we extracted profiles below seismic stations. All velocity-depth profiles were corrected for sediment thickness and truncated at the depth of the seismic Moho, yielding crustal seismic velocity as a function of sub-basement depth. Lastly, all velocity-depth profiles were combined into a single data set, and lower- and upper-limit envelopes were derived using Generic Mapping Tools (GMT) software (Wessel and Smith, 1998).

It could be argued that in addition to crustal ensembles, it would be useful to derive an average mantle structure to be used as reference for the assessment of serpentinization occurring in the oceanic mantle and at deep-sea trenches. However, the crust is reasonably isotropic, and when older than ca. 100 ka, it shows the same properties as mature crust several millions of years old (e.g., Purdy and Detrick, 1986; Grevemeyer et al., 1998; Holmes et al., 2008). In contrast, upper mantle is highly anisotropic, with velocities ranging from ~7.7 km/s to 8.6 km/s (e.g., Hess, 1964), and mantle structure indicates strong age-dependent changes, probably due to elevated temperatures and the presence of partial melt characterizing lithosphere younger than ca. 10 Ma (e.g., Grevemeyer et al., 1998). We therefore restrict the calculation of ensembles to crustal layers of oceanic plates.

In Figure 5 we compare our ensemble to ensembles from White et al. (1992). We would like to note that we used constraints from wide-angle reflections from the crust-mantle boundary to discriminate between crustal and

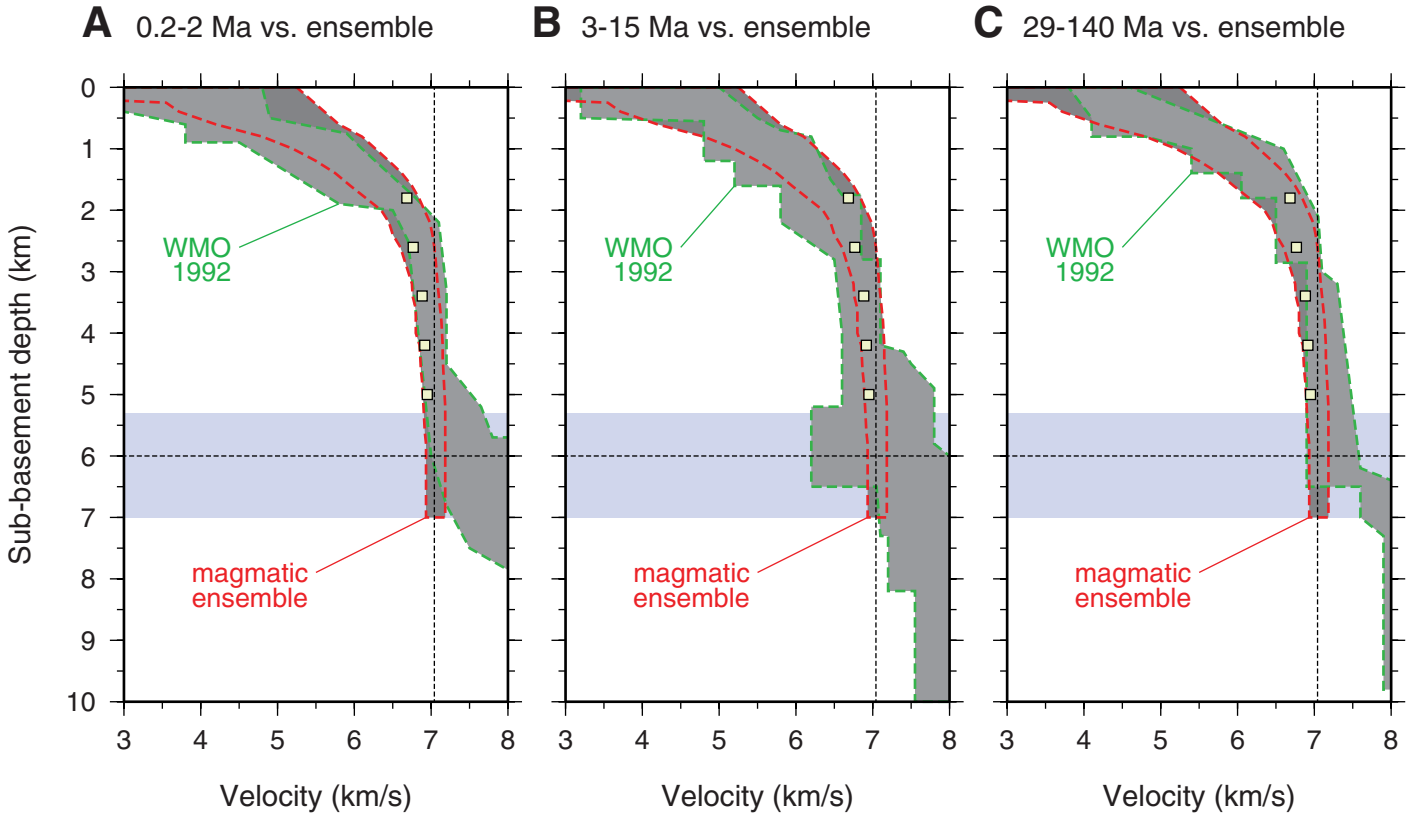

Figure 5. Pacific velocity-depth estimates from White et al. (1992) (WMO1992) versus our magmatic crust ensemble. (A) Magmatic ensemble versus 0.2–2 Ma crust of White et al. (1992). (B) Magmatic ensemble versus 3–15 Ma crust of White et al. (1992). (C) Magmatic ensemble versus 29–140 Ma crust of White et al. (1992). Yellow squares are estimates of lower-crustal velocity from Carlson and Miller (2004). Blue area marks variation in crustal thickness found in the velocity-depth profiles. Dashed lines as in Figure 4.

mantle velocity. For the ensembles, we used only data with the base of crust defined by wide-angle Moho reflections. In contrast, the White et al. (1992) compilation possibly included both crust and mantle. Further, due to their 1-D interpretation and the fact that their synthetic seismogram modeling caused in some cases thick crust-mantle transition zones, it is rather difficult to discriminate between crust and mantle in the White et al. (1992) ensembles. For discussion and classification, we concentrate on lower-crustal velocities, as mantle velocities might be affected by a suite of processes, including age, temperature, hydration, or basaltic melt frozen in the mantle.

In addition, we derived an ensemble for Pacific crust >100 km away from trenches (Fig. 6; Table S4 [footnote 1]), characterizing oceanic crust flooring the Pacific Basin. The Pacific ensemble includes a wide range of geographical settings, including young crust sampled off-axis at the East Pacific Rise, and mature crust from the eastern, southwestern, and northwestern Pacific. Last, for comparison and discussion, we also derived ensembles for young slow-spreading crust (Fig. 7; Table S5 [footnote 1]), discriminating between segment centers and segment ends. However, while the magmatic crust ensemble and Pacific crust ensemble include a wide range of crustal ages, the ensembles for Atlantic slow-spreading crust are based on crustal ages of <10 Ma.

The Magmatic Crust Ensemble

The new magmatic crust ensemble includes data from the Pacific (Grevemeyer et al., 1998; Canales et al., 1998, 2003; Oikawa et al., 2010; Moscoso et al.,

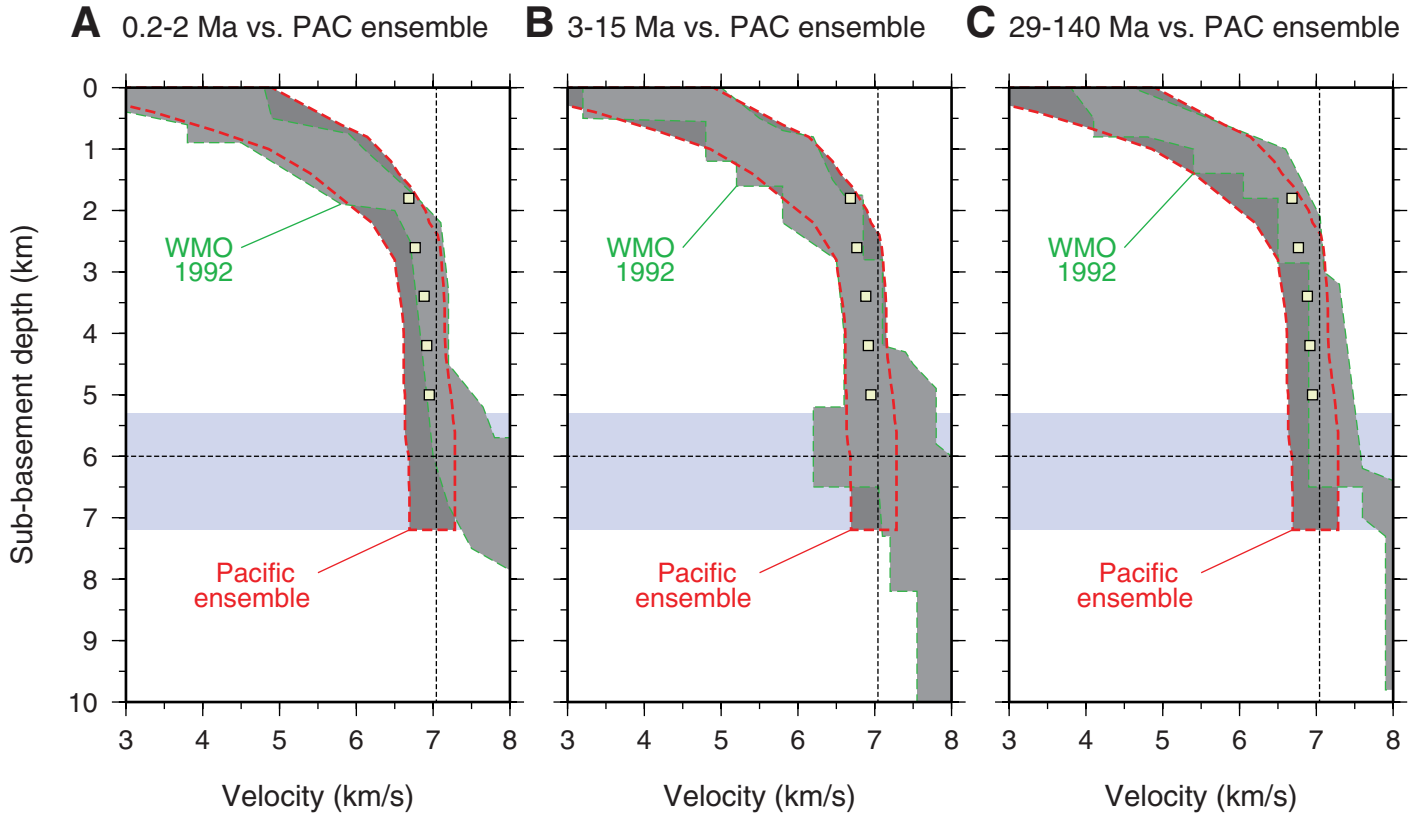

Figure 6. Pacific velocity-depth estimates from White et al. (1992) (WMO1992) versus our Pacific crust (PAC) ensemble. (A) Pacific ensemble versus 0.2–2 Ma crust of White et al. (1992). (B) Pacific ensemble versus 3–15 Ma crust of White et al. (1992) (C) Pacific ensemble versus 29–140 Ma crust of White et al. (1992). Yellow squares are estimates of lower-crustal velocity from Carlson and Miller (2004). Blue area marks variation in crustal thickness found in the velocity-depth profiles. Dashed lines as in Figure 4.

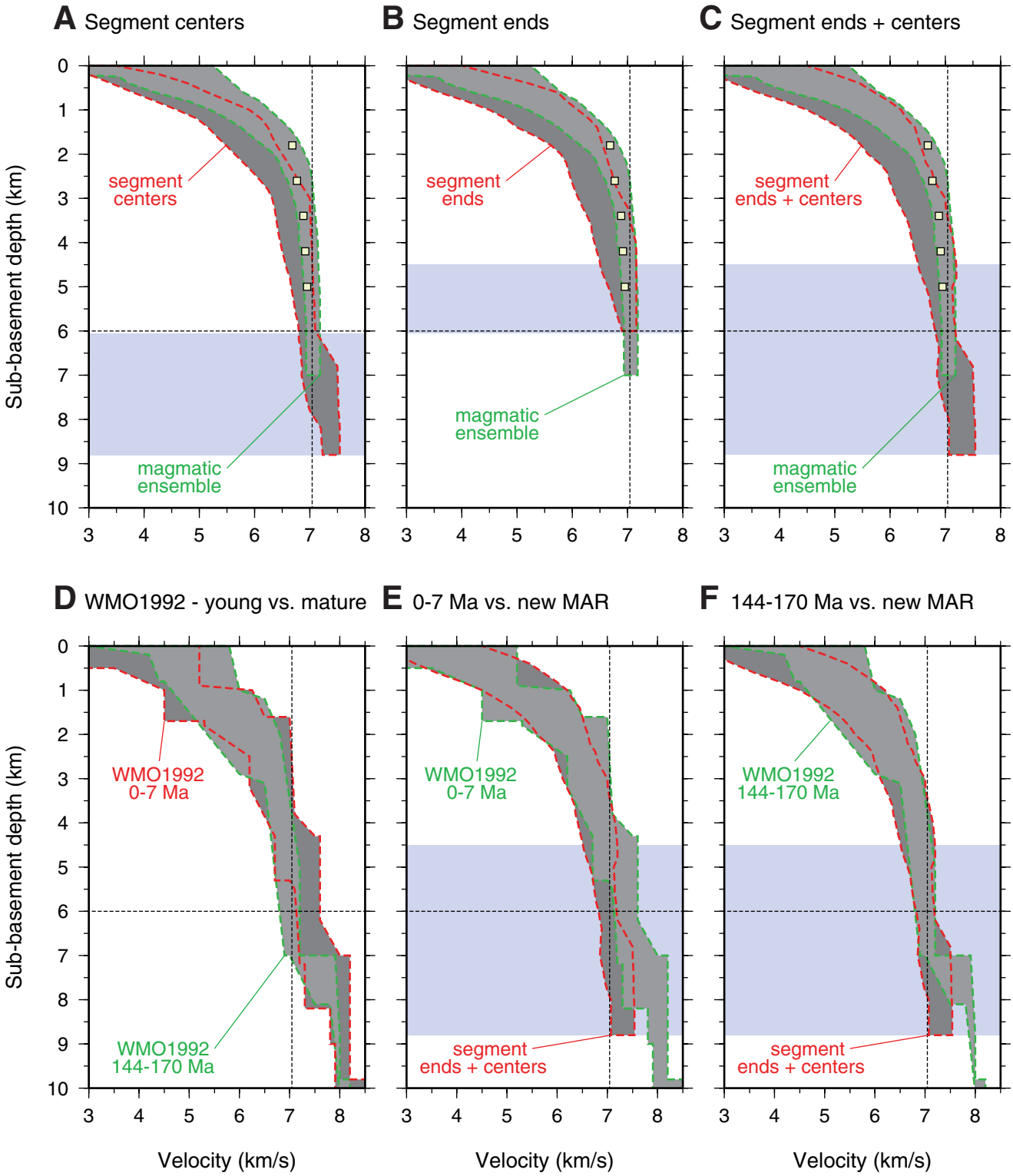

Figure 7. Velocity-depth estimates for slow-spreading ridge ensembles. (A) Segment centers versus magmatic crust ensemble. (B) Segment ends versus magmatic crust ensemble. (C) Combined slow-spreading ridge versus magmatic crust ensemble. (D) White et al. (1992) (WMO1992) young (0–7 Ma) versus mature (144–170 Ma) Atlantic crust ensemble. (E) Our combined slow-spreading ridge versus young Atlantic White et al. ensemble. (F) Our combined slow-spreading ridge versus mature Atlantic White et al. ensemble. New Mid-Atlantic Ridge (MAR) indicates our ensemble for segment centers and segment ends from the MAR. Blue areas mark variation in crustal thickness found in the velocity-depth profiles. Dashed lines as in Figure 4.

2011) and Indian Oceans (Grevemeyer et al., 2001; Holmes et al., 2008) formed at spreading rates of >65 mm/yr and ranging in age from young (ca. 0.5 Ma) to Jurassic-aged crust. When compared to the structure revealed by White et al. (1992) for the Pacific Basin (Fig. 5), we observe very similar features like a high-gradient upper crust and a low-gradient lower crust. However, the new ensemble shows considerably less scatter and provides a very narrow range of lower-crustal velocity, ranging from 6.93 to 7.18 km/s. Compared to 0.2–2 Ma crust of White et al. (1992), the velocity structure is similar, although the Moho transition zone is not apparent in the new model. However, White et al. (1992) showed for 3–15 Ma crust distinctively slower velocities of <6.9 km/s in the lower crust, and for 29–140 Ma seafloor, velocities of >7.3 km/s. Crustal thickness from the experiments chosen for the magmatic crust ensemble ranges from 5.3 to 7.0 km, whereas White et al. (1992) provided for Pacific extremal bounds of 4.9–7.9 km.

Drilling into lower-crustal rocks at tectonic windows allowed measurement of the seismic velocity of gabbroic rocks at a pressure of 200 MPa in the laboratory (e.g., Carlson and Miller, 2004), mimicking in situ conditions of the lower crust. Seismic velocities are generally in the range of 6.7–7.0 km/s, and velocity shows an increase with depth. Further, hardly any sample provided velocities faster than 7.2 km/s. Therefore, measurements on rock samples generally fall into the range of velocities of the magmatic crust ensemble, neither supporting the slow values of White et al. (1992) found in 3–5 Ma crust nor supporting fast velocities (>7.3 km/s) of White et al. (1992) found in 29–140 Ma crust. Average lower-crustal velocities obtained by Carlson and Miller (2004) are shown as yellow squares in Figures 4–7.

The Pacific Crust Ensemble

The ensemble for the Pacific Ocean includes the Pacific data used for the magmatic crust ensemble and additional data that deviate by >1% from 7.05 km/s or by >1 km from a mean thickness of 6 km. The ensemble, however, does not include any crust formed in western Pacific back arcs or near hotspots. With respect to the magmatic crust ensemble, the most prominent discrepancy occurs in the western Pacific and at the East Pacific Rise near 5°S. For example, data sampling the structure of the northwestern Pacific off the Kurile Trench (>100 km from the trench axis) provide seismic velocities of <6.9 km/s in the lower crust (Fujie et al., 2013). A similar type of crust was sampled off the Tonga Trench (>100 km from the trench axis and >100 km from the Louisville seamount chain; Contreras-Reyes et al., 2010). In contrast, crust >30 km away from the Quebrada and Gofar transform faults at the northernmost southern East Pacific Rise near 5°S showed lower-crustal velocities of >7.2–7.3 km/s (Roland et al., 2012). However, overall the Pacific crust ensemble displays a similar type of structure when compared to the magmatic crust ensemble (Fig. 8A), but lower-crustal rocks showed a wider range of velocities of 6.69–7.3 km/s.

The Slow-Spreading Crust Ensembles

The ensemble for the velocity structure of slow-spreading ridges has been divided into segment ends and segment centers. The discrimination has been driven by the observations that crustal thickness varies as a function of distance along the ridge crest and was first observed along the southern Mid-Atlantic Ridge in gravity field data corrected for density contrasts at the seabed and at Moho depth, called mantle Bouguer anomalies (Kuo and Forsyth, 1988; Tolstoy et al., 1993), and later confirmed by seismic studies (e.g., Canales et al., 2000a; Hooft et al., 2000; Dannowski et al., 2011). The process of focused mantle upwelling may also occur at intermediate- and fast-spreading ridges, but its effect is much smaller (e.g., Canales et al., 2003). When segment centers (Canales et al., 2000a; Hooft et al., 2000; Planert et al., 2009; Dannowski et al., 2011) and ends (Canales et al., 2000a, 2000b; Planert et al., 2009; Dannowski et al., 2011) are compared to the magmatic crust ensemble, the most prominent feature of the slow-spreading crust ensembles is a much wider range of velocities at mid- and lower-crustal levels (Figs. 7A and 7B). However, the upper extremal bound of both the magmatic crust ensemble and slow-spreading crust ensembles match at a depth of 3–6 km, suggesting that in spite of the slower spreading rate, a homogeneous lower crust may still form. The fact that the slower extremal bound of the slow-spreading ensemble is shifted to much lower velocities when compared the magmatic ensemble may indicate that the lower crust along slow-spreading ridges suffer from tectonism and hence crustal-scale fracturing and faulting, increasing porosity and reducing seismic wave speed.

A striking feature occurs near the base of the crust at segment centers, where a lowermost crust with velocities of >7.2–7.3 km/s (Canales et al., 2000a; Dannowski et al., 2011) occurs. Canales et al. (2000a) suggested that high velocities might be related to alternating layers of gabbro sills and dunites, features that were sampled in some ophiolites (Karson et al., 1984). With respect to crustal thickness, segment centers range from 6 km to >8.5 km, and segment ends have 4.5–6-km-thick crust.

In comparison to White et al. (1992), the overall trend of the slow-spreading crust ensembles is similar (Figs. 7D to 7F). However, 0–7 Ma crust from White et al. (1992) showed lower-crustal velocities of 7.2–7.6 km/s at 4–7 km depth (which has been called Moho transition zone), a feature not observed in modern surveys. Surprisingly, even the oldest crust of 144–170 Ma of White et al. (1992) matches the mid- and lower-crustal velocities of the Atlantic crust ensemble derived for crust <10 Ma, supporting that crustal accretion was reasonably constant over time.

SEISMIC STRUCTURE AT DEEP-SEA TRENCHES

The observation that bend faulting is an evolutionary process affecting the volatile flux into the deep Earth's interior has been established during the last ~10 years. The first systematic surveys were conducted offshore of northern

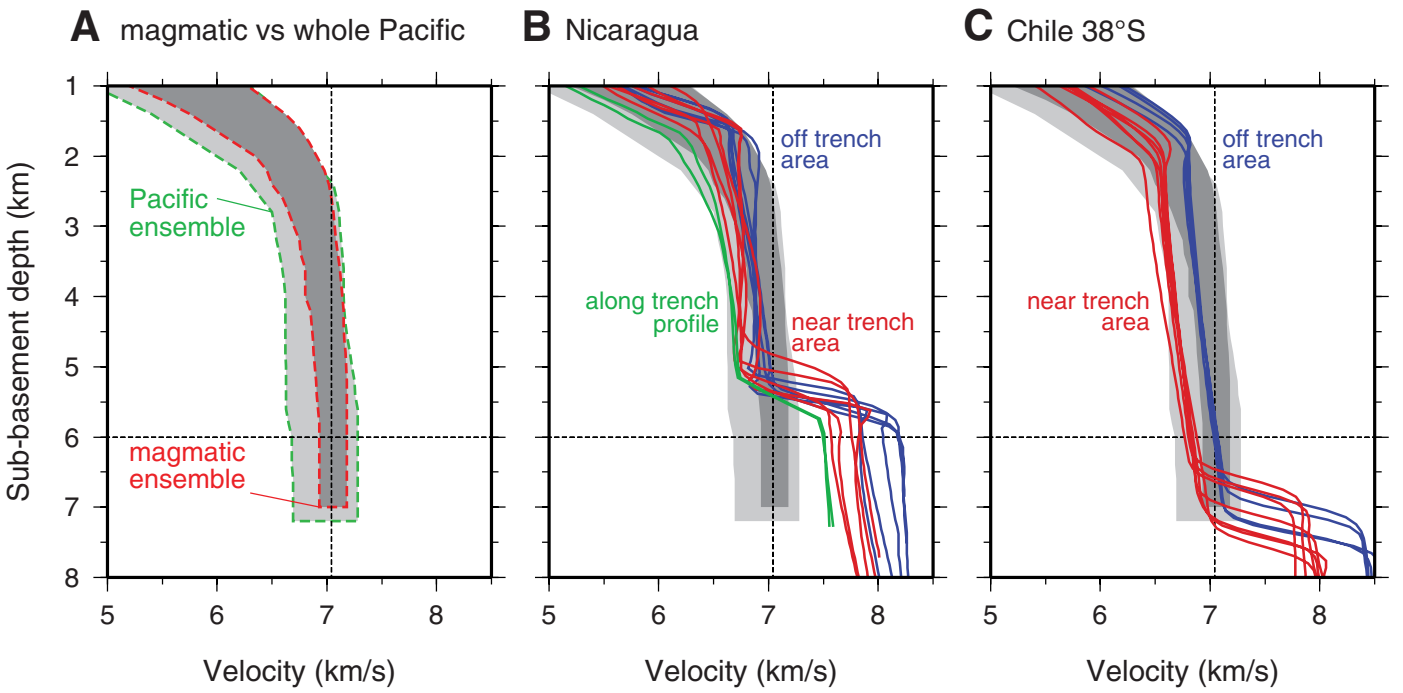

Figure 8. Effects of bend faulting on velocity-depth profiles. (A) Magmatic crust versus Pacific crust ensemble. (B) Magmatic crust and Pacific crust ensembles versus velocity-depth profiles from offshore of Nicaragua; blue and red indicate off-trench and near-trench velocities, respectively (Ivandic et al., 2008); green indicates trench-parallel velocity structure (Ivandic et al., 2010). (C) Magmatic crust and Pacific crust ensembles versus velocity-depth profiles from offshore of Chile at 38°S; blue and red indicate off-trench and near-trench velocities, respectively (Contreras-Reyes et al., 2008). Dashed lines as in Figure 4.

Costa Rica and Nicaragua, where a ca. 24 Ma oceanic lithosphere is subducted at 9.1 cm/yr under Middle America. High-resolution bathymetric mapping of the incoming plate shows that the plate is pervasively fractured across most of the ocean-trench slope (Fig. 9). Seafloor-spreading anomalies strike approximately parallel to the trench axis; thus, the orientation of the tectonic fabric formed at the spreading center seems to govern the amount of faulting. Some of the faults can be tracked in the multibeam bathymetry for at least 50 km along the trench, and multi-channel seismic reflection data suggest that they cut ~18–20 km into the plate (Ranero et al., 2003). The outer rise is also affected by large normal-faulting earthquakes with magnitudes of M_w = 5.5–6.3, occurring in faults ~50 km long that reach 5–10 km down dip (Lefeldt and Grevemeyer, 2008).

Offshore of Nicaragua, the first systematic wide-angle seismic data set in a trench was collected in 2003, surveying the effect of plate bending and hydration in the trench–outer rise (Grevemeyer et al., 2007; Ivandic et al., 2008). Indeed, as deduced from seismic reflection imaging (Ranero et al., 2003) and heat flow anomalies (Grevemeyer et al., 2005), bend faults were shown to govern systematic changes in the structure of the incoming plate (Fig. 10). Distinct features are the reduction of lower-crustal P-wave velocities from values of ~6.95 km/s ~100 km away from the trench to 6.7 km/s in the trench axis (Figs. 10A, 8B, and 11). Even more pronounced are changes of the lower-crustal S-wave velocities (Ivandic, 2008), decreasing from 3.8 km/s at the outermost trench slope to 3.4 km/s in the trench axis (Figs. 10B and 11). In consequence, the Vp/Vs ratio increases with decreasing distance from the trench axis (Fig. 11). This feature is typical of increased rock fracturing under water-saturated conditions (Popp and Kern, 1994; Wang et al., 2012), supporting the observation that the number of faults and fault throw increase approaching the Nicaraguan trench axis (Ranero et al., 2003).

In concert with crustal velocity, the seismic velocity of the uppermost mantle decreases from 8.2 km/s to 7.6 km/s for P-waves and 4.7 km/s to 4.2 km/s for S-waves (Fig. 11). Velocity reduction may indicate a degree of serpentinization of ~10%–12% (e.g., Christensen, 1972, 2004). However, the assessment of the

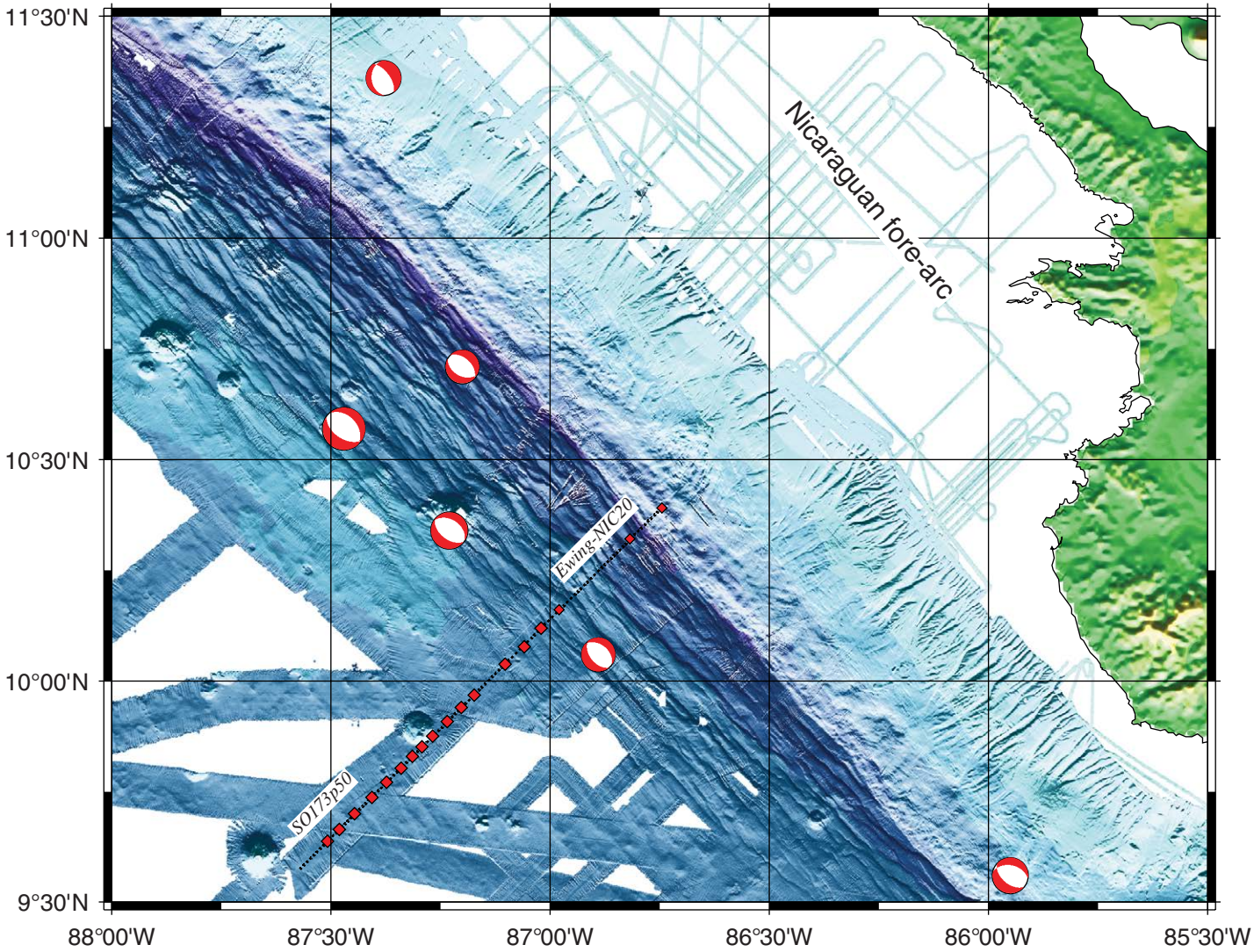

Figure 9. Bathymetric map of bend faulting offshore of Nicaragua. Note the trench-parallel stairway-like fault structures in the trench–outer rise. Focal mechanisms of normal-faulting earthquakes are solutions from the Global Centroid Moment Tensor Project (http://www.globalcmt.org). Seismic profile and ocean-bottom seismometers used by Ivandic et al. (2008) are shown by the black line and red squares. The line reported by Ivandic et al. (2008) was a composite line, combining shots and ocean-bottom seismometers from the two profiles SO173p50 and Ewing-NIC20. Figure is modified from Ivandic et al. (2008). Blue colors indicate depth below sea level and green colors above sea level.

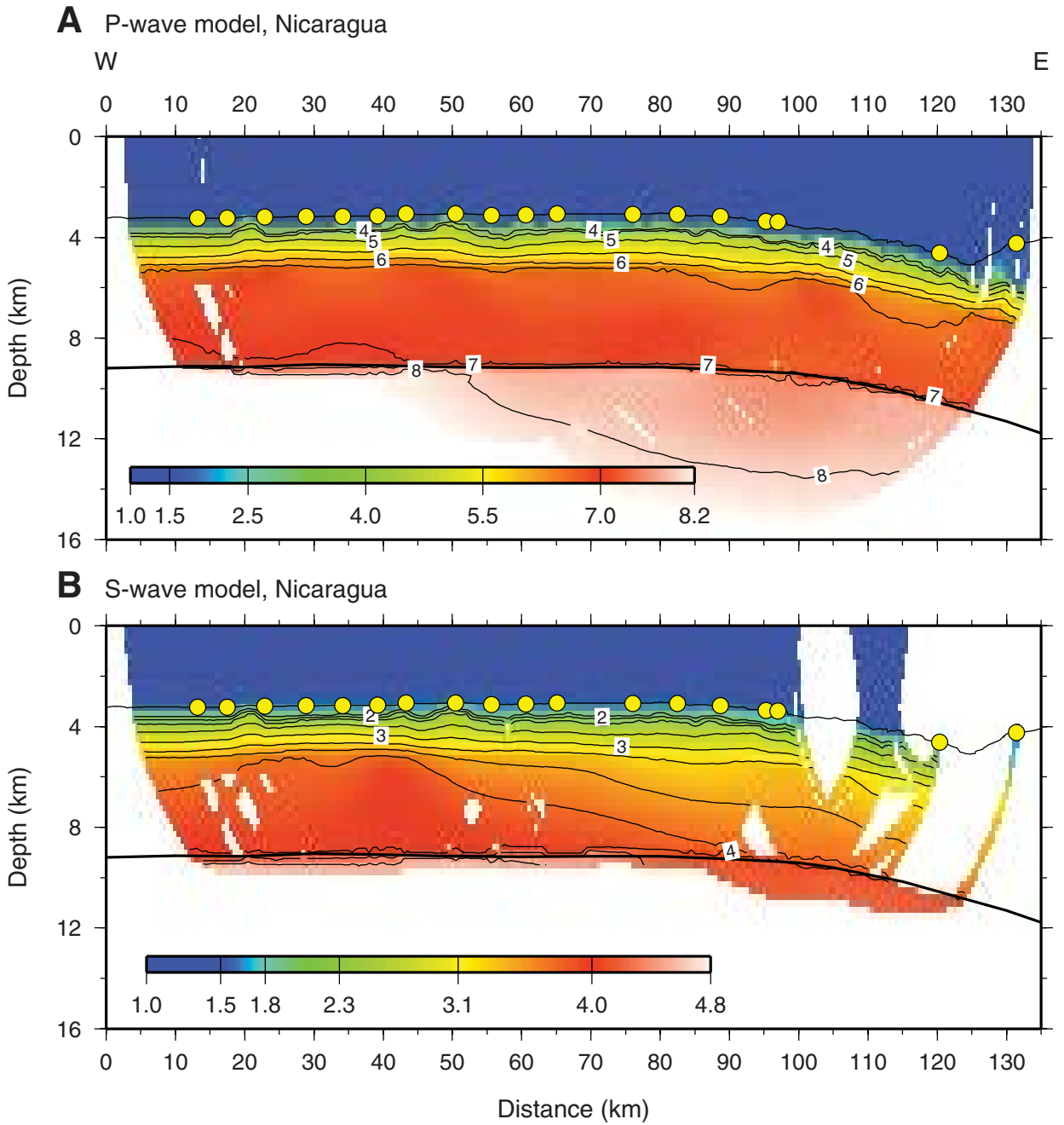

Figure 10. Tomographic velocity structure along composite profile SO173p50–Ewing-NIC20, offshore Nicaragua (see Fig. 9 for location). (A) P-wave tomography (Ivandic et al., 2008). (B) S-wave tomography (Ivandic, 2008). Yellow dots indicate location of ocean-bottom seismometers on the seafloor. S-wave velocity (Vs) is related to that of P-wave velocity (Vp) by Vs = Vp / 1.75; Vs > 1.6 km/s.

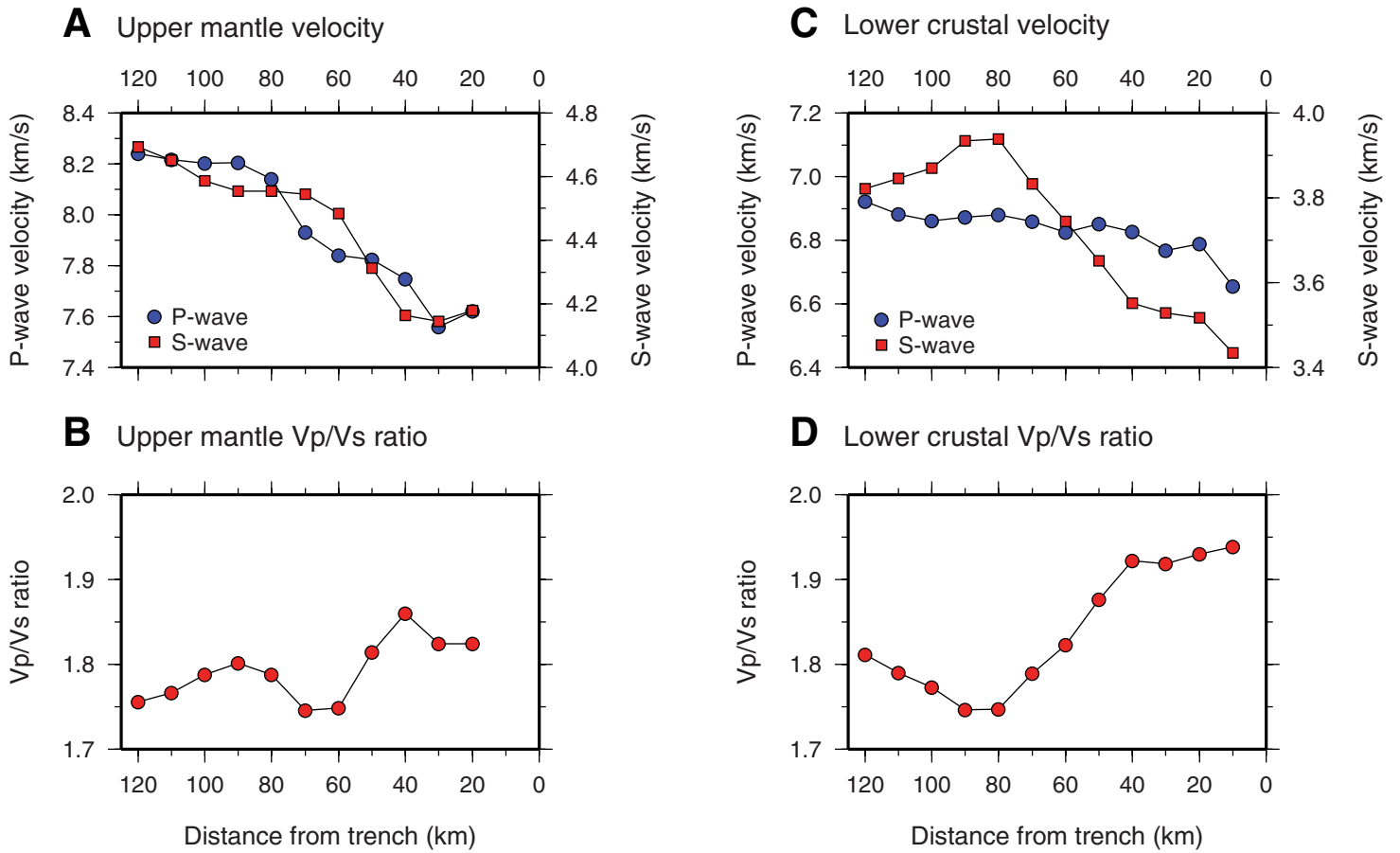

Figure 11. Velocity results from composite profile SO173p50–Ewing-NIC20, offshore Nicaragua (Fig. 9), as a function of distance from the trench axis. (A) Upper mantle velocity. (B) Upper mantle P-wave to S-wave velocity ratio (Vp/Vs). (C) Lower crustal velocity. (D) Crustal Vp/Vs ratio.

degree of serpentinization is rather difficult, as the mantle shows a large degree of anisotropy (e.g., Hess, 1964; Christensen, 2004), while most empirical relationships between seismic velocity and serpentinization assume isotropic conditions (e.g., Christensen, 1972). Consequences are perhaps best explained by a number of trench-parallel profiles shot offshore of Nicaragua. Tomographic constraints from Ivandic et al. (2010) and van Avendonk et al. (2011) indicated seismic velocities in the mantle as low as 7.4–7.5 km/s and 7.0–7.2 km/s, respectively. Assuming isotropic conditions and a commonly used relationship between Vp and serpentinization of $Vp = 8 - 3.1\phi$, where ϕ is the amount of serpentinization ranging from 0 (0%) to 1 (100%), would yield 16%–18% of serpentinization for the Ivandic et al. (2010) and 20%–30% for the van Avendonk et al. (2011) study. However, both studies ran parallel to the trench and hence samples in the slow direction of mantle anisotropy. Unfortunately, here there are no available trench-parallel data of crust not yet affected by bend faulting. Offshore of Chile near 34°S, Moscoso and Grevemeyer (2015) sampled velocities of 8.2 km/s and 7.8 km/s in the fast and slow directions, respectively. Offshore of Nicaragua and away from the bend-faulting area, Ivandic et al. (2008) also observed a mantle velocity of 8.2 km/s in the fast direction. Assuming that the degree of anisotropy off of Nicaragua is roughly similar to the one observed off of Chile would lower the P-wave velocity anomaly by ~0.2 km/s and the amount of serpentinization to 10%–12% for Ivandic et al. (2010) and 18%–20% for van Avendonk et al. (2011), respectively. However, other factors

may contribute to the reduction in upper mantle velocity, including porosity created by bend faulting, although the amount of feasible porosity in the mantle is unclear due to both porosity-closing effect of pressure at 6–8 km depth and volumetric increase accompanying serpentinization.

To further discriminate between dry mantle and serpentinized mantle, Vp/Vs ratios might be extremely useful. It has long been recognized in laboratory data that with an increasing degree of serpentinization, the Vp/Vs ratio increases, too (Christensen, 2004), and hence a Vp/Vs ratio of >1.8 may indicate serpentines. In Figure 12, we examine the mantle properties found offshore of Nicaragua and plot Vp (Ivandic et al., 2008) versus Vs (Ivandic, 2008) to yield Vp/Vs ratios. Indeed, the data support two clusters. One indicates dry conditions with a Vp/Vs < 1.8, and the second one has Vp/Vs > 1.8, supporting

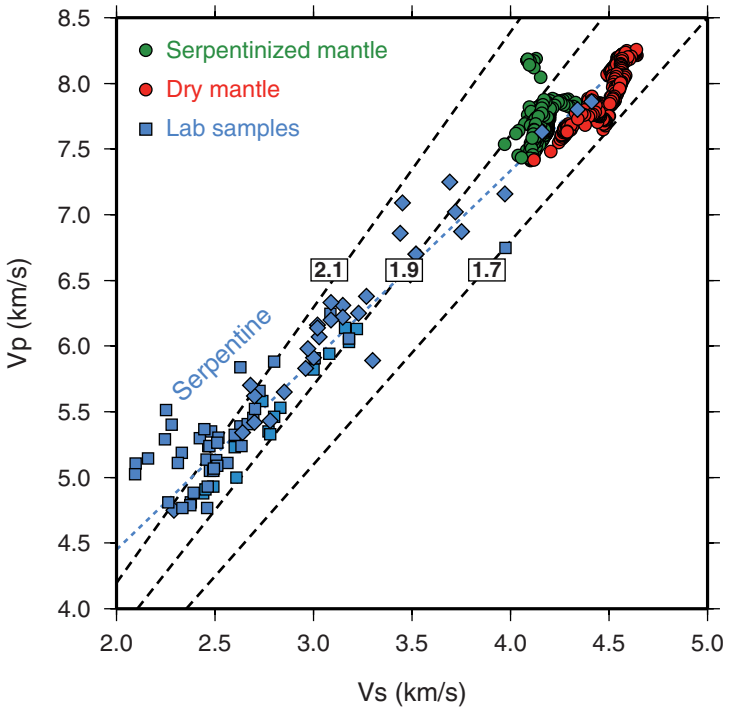

Figure 12. P-wave (Vp) versus S-wave (Vs) velocity derived from laboratory study (blue squares; Christensen, 1972, 2004), and constraints from composite profile SO173p50–Ewing-NIC20, offshore Nicaragua (red and green dots; Fig. 9). Dashed black lines indicates Vp/Vs ratios as indicated by label. Blue dotted line running through lab samples has been interpolated by Carlson and Miller (1997). Note, seismic refraction data support basically two clusters: Vp/Vs < 1.8 (red) and Vp/Vs > 1.8 (green), which are interpreted to indicate dry and serpentinized peridotites, respectively.

hydration. This finding clearly supports that mantle becomes progressively serpentinized when approaching the trench axis.

The patterns first studied and observed across northern Chile and the Middle America Trench off of Nicaragua are now recognized to be a global phenomenon, including systematically decreasing seismic velocities of crust and mantle when approaching a deep-sea trench (Fig. 13). In Table 1 and Figure 14, we summarize constraints from a number of different subduction zones (for location of areas in map view, see Fig. 14), including most of Chile, Cascadia, Alaska, Tonga, and Java. Indeed, seismic tomographic imaging at subduction zones showed trench lower-crustal velocities of 6.5–6.8 km/s, which are clearly reduced when compared to our new reference model (magmatic crust ensemble) with velocities of 6.9–7.1 km/s, or to crust sampled further away from the trench in the outer rise (Fig. 14B). Similar features occur in the mantle (Fig. 14C): in the vicinity of deep-sea trenches, upper mantle velocities are in the order of 7.6–7.7 km/s with extreme bounds of 7.0 km/s (Nicaragua, slow direction; van Avendonk et al., 2011) and ~8.1 km/s (Cascadia, fast direction; Horning et al., 2016). Further, except for the Cascadia survey, all profiles extending from the trench into the outer rise show an evolutionary process, with mantle velocities being faster in the outer rise and slower near the trench axis, supporting serpentinization. In general, the anomalies are reasonably independent on lithospheric age. However, the youngest lithosphere surveyed off Cascadia did not provide any evidence for serpentinization, even though a clear and systematic reduction in lower-crustal velocity toward the trench axis has been observed (Figs. 13B and 14B). However, Cascadia is a young plate where mantle temperature may be too high for serpentinization (Horning et al., 2016) even if faulting provides mantle-reaching water conduits.

DISCUSSION

Crustal Ensembles and Indications for Hydration

In marine wide-angle seismology, crustal ensembles are frequently used to characterize and compare domains to previously found constraints. However, over the last decades, we have learned that seafloor spreading does not create one "typical oceanic crust", but that oceanic crust varies profoundly with spreading rate or its setting. This is perhaps best indicated by the variability of crustal thickness as a function of age and spreading rate, as displayed in Figure 2. We therefore believe that the newly defined "magmatic crust ensemble" model with it reasonably tight extremal bounds based on modern seismic data may provide an improved reference to compare and assess processes shaping the oceanic crust rather than characterizing crust by its geography.

When we compare our magmatic crust ensemble to the Pacific Ocean ensemble, we observe that large areas in the southwestern and northwestern Pacific (Contreras-Reyes et al., 2010; Fujie et al., 2013) show a lower-crust velocity reduction of ~0.2 km/s, i.e., the lower extremal bound is shifted to slower velocities (Fig. 8A). In comparison, areas affected by bend faulting

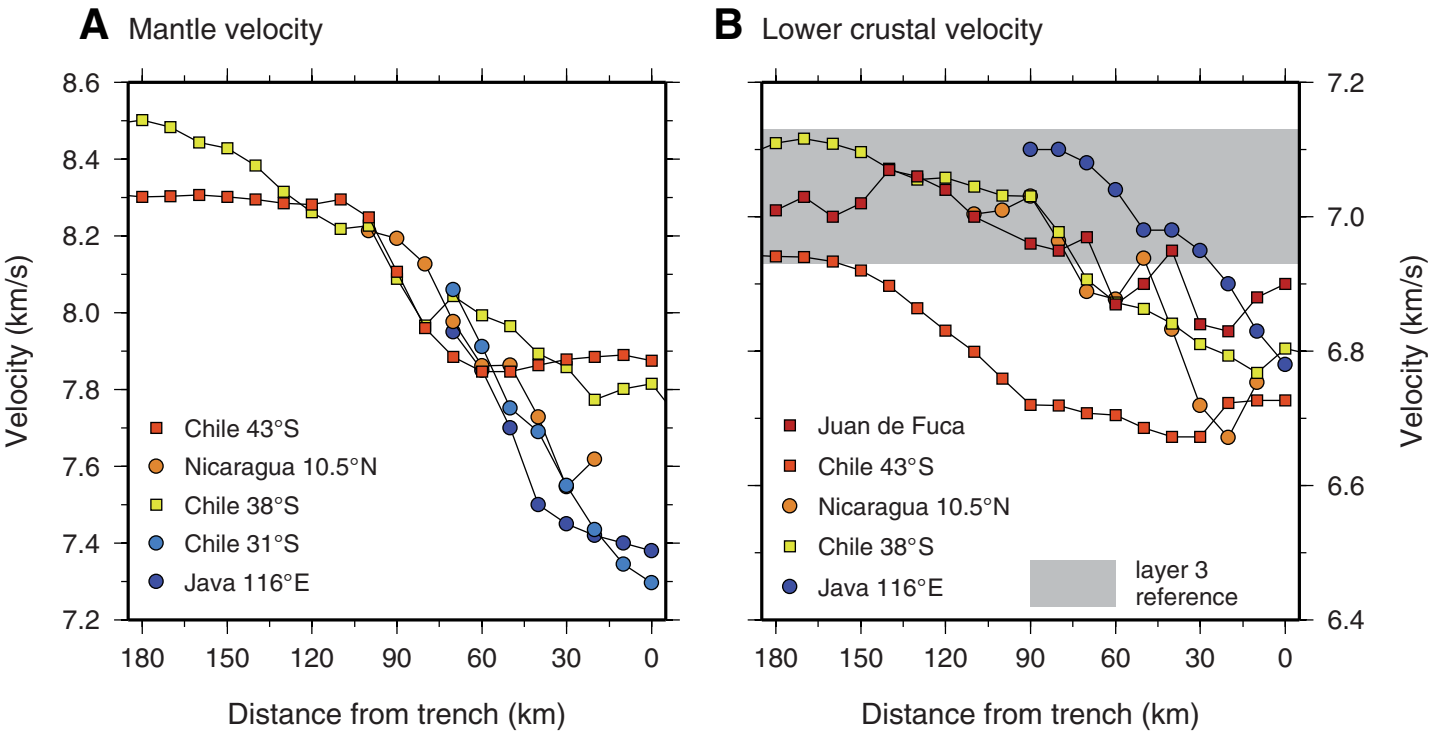

Figure 13. Compilation of results from seismic profiles approaching deep-sea trenches. (A) Mantle velocity. (B) Lower crustal velocity. Note, velocity reduction in the vicinity of the trench is a global phenomenon, indicating alteration and hydration. Data sources: Chile 43°S—Contreras-Reyes et al. (2007); 38°S—Contreras-Reyes et al. (2008); 31°S—Contreras-Reyes et al. (2014); Nicaragua—Ivandic et al. (2008); Java—Planert et al. (2010); Juan de Fuca—Horning et al. (2016).

(Figs. 8B and 8c) show a very similar velocity-depth structure. One interpretation might be that even areas within 100–500 km of a trench might be affected by bend faulting. Hunter and Watts (2016) showed that for old and hence rigid lithosphere, like at Tonga (>80 Ma) and Kurile (ca. 110 Ma), plate bending occurs several hundreds of kilometers away from the trench. It might be reasonable to hypothesize that microfracturing related to bending controls the reduced lower-crustal velocities found in the western Pacific Ocean. However, one could also speculate that parental mantle composition at the time of lithospheric formation was different, affecting bulk crustal composition and hence seismic velocities.

The new magmatic crust ensemble is a useful reference model when surveying trench-parallel profiles to delineate the effects of bend faulting. For example, off of Nicaragua, van Avendonk et al. (2011) and Ivandic et al. (2010) observed lower-crustal velocities of ~6.6 km/s. These values match the extremal bound of the Pacific field, but are significantly reduced compared to the magmatic crust ensemble (Fig. 8B) highlighting the impact of bend faulting.

A striking feature of the slow-spreading crust ensembles was, with respect to the magmatic crust ensemble, the observation that the slower extremal bound is shifted to lower velocities. As for the old-crust west-Pacific ensemble, a likely explanation is the occurrence of deep faulting, albeit in slow-spreading crust, faulting occurs at the mid-ocean ridge. Faulting and accompanying fracturing increases bulk porosity, decreasing seismic wave speed. Newly created porosity and faulting provide pathways into the upper and lower crust and hence promote hydration, as envisioned for bend faults. Carlson and Miller (2004) noted that even if cracks are not present, on average, gabbros with velocities typical of seismic layer 3 (6.7–7.0 km/s) contain 5%–15% alteration products, including 5%–15% amphibole and 0%–5% phyllosilicates. It might therefore be reasonable to assume that reduced lower-crustal velocities indicate an even higher degree of cracking and alteration, suggesting that, if subducted, slow-spreading lithosphere would be a major agent to transfer large amounts of bound water into the Earth's interior. Today, however, subduction of slow-spreading lithosphere occurs only at two narrow settings, the

TABLE 1. COMPILATION OF SEISMIC VELOCITY STRUCTURE FROM SEISMIC TOMOGRAPHY AT TRENCH–OUTER RISES

Area	Age (Ma)	Fabric*	Sediment thickness (km)	Vp mantle, outer rise (km/s)†	Vp mantle, trench (km/s)	Degree of serpentinization (%)§	Vp lower crust, outer rise (km/s)	Vp lower crust, trench (km/s)	Reference
1. Chile 23.5°S	53	2	<0.2	-/- (3)	~7.6	~12	7.1	6.8–6.9	Ranero and Sallarès, 2004
2. Chile 31°S	42	2	<0.2	8.1 (3)	7.6–7.7	10–12	7.2	~6.8	Contreras-Reyes et al., 2014
3. Chile 32°S	41	2	0.1–0.2	-/- (3)	~7.8	5–6	7.0	6.8–7.0	Contreras-Reyes et al., 2015
4. Chile 34°S	35	2	0.2–0.4	7.8 (1)	7.5–7.8	6–16	7.1	6.8–6.9	Moscoso and Grevemeyer, 2015
5. Chile 38°S	30	2	0.4–2.4	8.4 (3)	7.8–7.9	4–6	7.2	6.7–6.9	Contreras-Reyes et al., 2008
6. Chile 43°S	15	1	0.6–2.4	8.3 (2)	7.8–7.9	4–6	7.0	6.7–6.8	Contreras-Reyes et al., 2007
7. Nicaragua 10°N	24	1	0.4–0.6	-/- (2)	7.4–7.5	16–18	-/-	6.4–6.6	Grevemeyer et al., 2007
8. Nicaragua 10.25°N	24	1	0.4–0.6	8.2 (2)	7.6–7.7	10–12	6.95	6.7–6.8	Ivandic et al., 2008
9. Nicaragua 11°N	24	1	0.4–0.5	-/- (1)	7.4–7.5	16–18	-/-	6.6–6.8	Ivandic et al., 2010
10. Nicaragua 9°–11°N	24	1	0.3–0.6	-/- (1)	7.0–7.2	20–30	-/-	6.6–6.7	van Avendonk et al., 2011
11. Tonga 24.5°N	80	2	0.1–0.4	-/- (1)	7.3–7.4	18–22	-/-	6.8–6.9	Contreras-Reyes et al., 2011
12. Cascadia 45°N	9	1	0.1–3	8-8.2 (2)	8.1–8.2	0	7.0–7.1	6.6–6.7	Horning et al., 2016
13. Alaska 160°W	53	1	0.4–0.6	8.25 (3)	7.7–7.8	6–10	6.6–6.7	~6.5	Shillington et al., 2015
14. Kuril 147°E	130	1	0.4–0.8	8.4 (2)	7.9–8.0	1–2	6.7–6.8	6.6–6.7	Fujie et al., 2013
15. Java 116°E	134	1	0.3–0.5	7.9 (3)	7.4–7.6	12–18	7.1	6.8–6.9	Planert et al., 2010
16. Java 119°E	157	1	0.5–0.6	7.8 (3)	7.4–7.5	16–18	7.05	~6.5	Planert et al., 2010

Notes: The numbered areas are shown in Figure 14. Age refers to crustal age; Vp is the P-wave velocity; -/- indicates that no data are available.
*Bend-fault fabric: 1—reactivated faults originally created at spreading axis; 2—newly created bend faults.
†Anisotropy shown in parentheses: 1—slow direction; 2—fast direction; 3—oblique.
§$Vp = 8 - 3.1\phi$, where ϕ is degree of serpentinization.

Antilles and South Sandwich arcs. Globally, the total length of active subduction zones is 44,450 km (Jarrard, 2003), indicating that the length of ~2000 km of slow-spreading crust subduction is a minor contribution to the return flow of water into the mantle. However, in the past, the return flow of water into the mantle may have been much larger, and will be in the future when the Atlantic Basin is closing.

Processes Controlling the Magnitude of Hydration at the Trench–Outer Rise

The review of wide-angle seismic data compared to the new model of crustal ensembles of seismic velocity as a function of depth provides strong evidence supporting that the oceanic plate going across the outer rise and trench is modified by an evolutionary deformation process driving alteration and hydration prior to subduction (Figs. 11, 13, and 14). However, the amount of hydration remain inadequately constrained. In particular, it is not yet fully evaluated how, in addition to hydration, faulting and cracking may cause decreasing crustal and upper mantle velocity.

We argue that the availability of seawater and its migration along bend faults is critical. Laboratory studies showed that in cracked formations, dry rocks display a decreasing Vp/Vs ratio with increasing amount of cracking, while water-saturated rocks exhibit an increasing ratio (Popp and Kern, 1994; Wang et al., 2012; Korenaga, 2017). The bend faulting area of Nicaragua shows increasing Vp/Vs ratios (Fig. 11D), supporting water-filled joints. The interpretation is supported by constraints from an active-source electromagnetic study, supporting water-filled cracks in the outer rise of Nicaragua (Naif et al., 2015). Further, increasing crustal Vp/Vs ratios have also been observed in the Kurile Trench, where Vp/Vs increases approaching the trench axis (Fujie et al., 2013). Thus, Vp/Vs ratios support that bend faults efficiently create pathways for seawater to flow into the crust and possibly into the mantle.

Global seismic surveys indicate decreasing mantle velocity when approaching deep-sea trenches (Fig. 14). The most popular interpretation would be that bend faulting and serpentinization control changes in seismic velocities. It might be interesting to note that it is generally assumed that serpentinization occurs throughout the uppermost mantle. However, assuming that serpentine is concentrated along fault zones, in contrast to a uniform distribution, reduced wave speed observed off Nicaragua can be explained by slowing from serpentinized joints, along with anisotropy inherited from the incoming upper mantle (Miller and Lizarralde, 2016). In consequence, estimates of bulk upper mantle hydration would be reduced from ~3.5 wt% for uniform serpentinization to as low as 0.33 wt% H_2O for serpentinization confined to fault zones (Miller and Lizarralde, 2016). Alternatively, Korenaga (2017) argued that crack porosity rather than hydration controls the velocity reduction at trenches, suggesting that bend faulting would not lead to substantial hydration of oceanic plates. However, laboratory studies showed that serpentines have high Vp/Vs ratios with respect to dry peridotite (Christensen, 2004), indicating that a Vp/Vs ratio of >1.8 sampled at the Nicaraguan trench (Figs. 11B and 12) supports hydration of mantle by serpentinization. In contrast, assuming that crack porosity is controlling the systematically increasing of Vp/Vs ratios would require

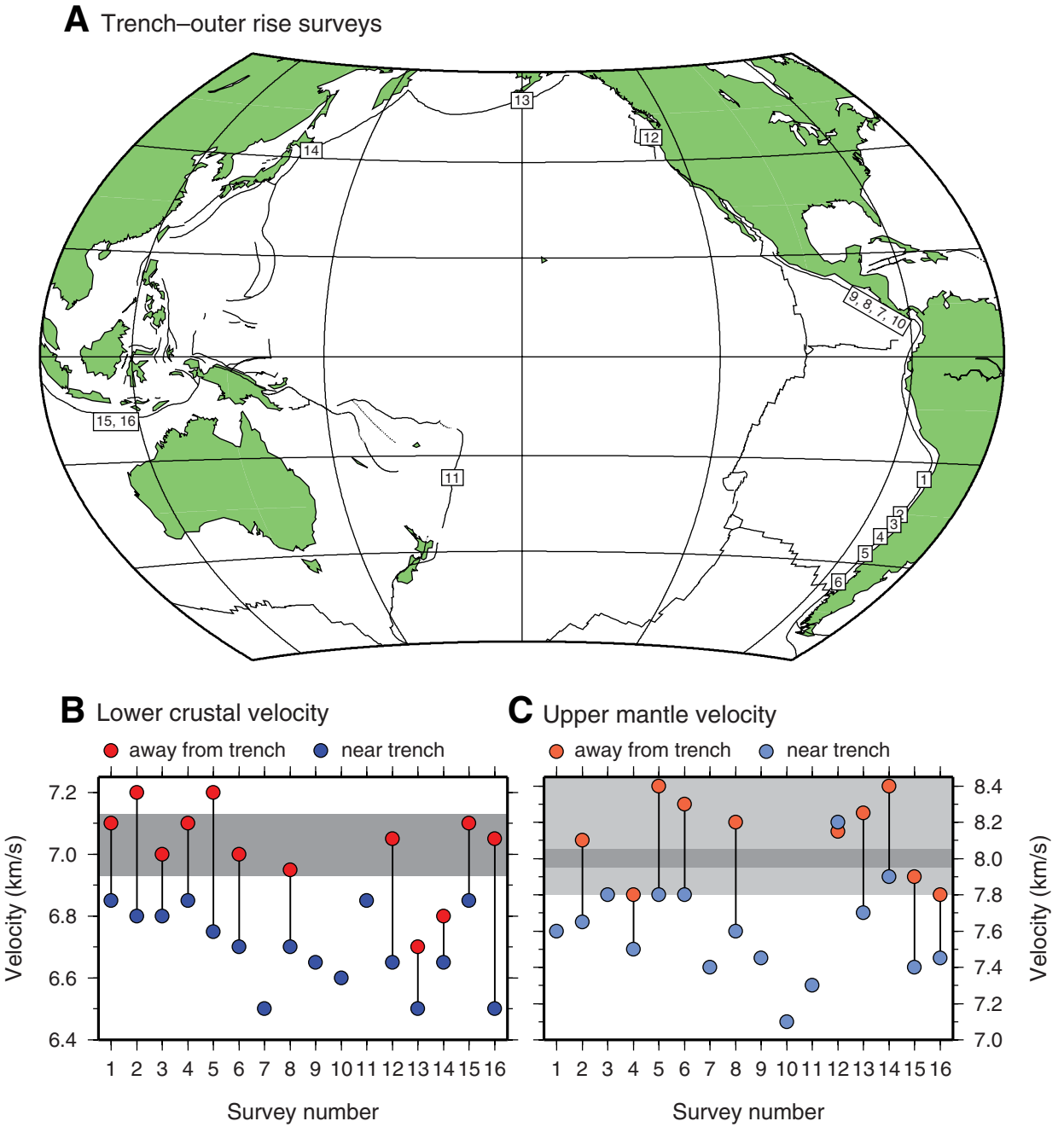

Figure 14. (A) Map view of seismic surveys conducted in the trench–outer rise. (B) Velocity in the lower crust sampled at trenches; gray area marks reference structure of oceanic crust. (C) Upper mantle velocity in the vicinity of trenches; light gray indicates fast and slow values of mantle velocity caused by anisotropy; dark gray indicates isotropic mantle. Note, lines linking colored circles indicate systematic reduction of seismic wave speed when approaching the trench. Data and sources are shown in Table 1.

an evolutionary change in aspect ratio of the porosity, which is difficult to envision.

Serpentinization only occurs when water is supplied to the mantle and temperatures are in the range of 100–400 °C (e.g., Martin and Fyfe, 1970). Cascadia is an end member where mantle is ~450 °C (Horning et al., 2016), i.e., too hot for serpentine formation to occur. Consequently, in the case of bend faulting, we should observe a crustal velocity anomaly, but the mantle should basically show normal mantle properties. Indeed, Cascadia displays a clear lower-crustal velocity anomaly (Figs. 13B and 14B), but velocity within the mantle remain unchanged (Fig. 14C), even though multi-channel seismic reflection data show that bend faults cut into the mantle (Horning et al., 2016). If faulting alone would explain the widespread observation of velocity reduction at trenches (e.g., Korenaga, 2017), Cascadia mantle should have reduced mantle velocities, but with 8.0–8.1 km/s velocities, Cascadia possibly has a dry mantle (Horning et al., 2016).

In addition to temperature appropriate for serpentinization (100–400 °C), dynamics of serpentinization itself may control the magnitude and distribution of hydration (Iyer et al., 2012). Most important is the dependence of reaction kinematics on temperature, showing that serpentinization is most effective at temperatures of ~270 °C, tapering off at higher and lower temperatures (Martin and Fyfe, 1970). Iyer et al. (2012) studied the relationship between reaction kinematics and hydration to show that hydration strongly depends on plate age and subduction rate, suggesting that both increasing lithospheric age and decreasing subduction rate enhance hydration. Further, reduction kinematics explains the occurrence of double seismic zones at Wadati-Benioff zones (Iyer et al., 2012), suggesting that serpentine formation reaches deeper into the mantle as plates mature.

A critical parameter for hydration is the availability of water. From hydrogeology studies, it is proposed that hydrothermal circulation is shut off when impermeable sediments blanket the basement (Stein and Stein, 1994). We therefore may expect that hydration may depend on trench fill. In southern Chile, Contreras-Reyes et al. (2007) observed that small conical seamounts could facilitate the flow of seawater into the igneous section of the incoming plate. However, analyzing the reduction of mantle velocity in trenches, there appears to be a dependence on the amount of trench fill (Table 1), suggesting that a setting where basement breaches the sediment at bend faults supports hydration. Thus, the magnitude of velocity reduction at the trench axis is smaller off of southern Chile (trench fill >2 km) when compared to Nicaragua, northern Chile, or Java (trench fill <500 m) (Fig. 13). It is therefore reasonable to suggest that trenches with little trench fill may globally contain a larger degree of hydration, while sediment-covered trenches would promote only moderate degrees of serpentinization.

A currently unconstrained process is the hydrological evolution of the underthrusting oceanic slab. The slab continues to bend to as much as 40–60 km depth as shown by abundant normal-fault earthquakes, and free water is available at all depths either from pore water at <~20 km or later from progressive dehydration of sediment and upper igneous crust hydrothermal minerals. Conceivably some of that water may find pathways into the slab and further extend the amount of hydration.

Processes Controlling the Maximum Depth of Infiltration of Water at the Trench–Outer Rise

All seismic data collected in subduction trenches show evidence for significant modification of the lithosphere prior to subduction (Figs. 8, 10, 11, 13, and 14). Yet, incorporation of water into oceanic plates before subduction is a poorly understood process. Forces controlling hydration of the plate in the trench–outer rise include plate bending and/or slab pull (Faccenda et al., 2009). Slab pull stresses might be periodically transferred into the trench–outer rise when sufficiently large subduction megathrust earthquakes unlock the plate interface (e.g., Ammon et al., 2008). The depth of fracturing by outer rise normal-fault earthquakes is usually not well constrained, but could potentially create deep paths for water percolation that might hydrate as deep as tens of kilometers into the mantle, restrained only by serpentine stability (Ranero et al., 2003). Yet, interpretation of deep intraplate mineral alteration remains speculative, because active-source seismic experiments have sampled only the uppermost few kilometers of mantle (Fig. 10), leaving the depth extent of anomalous velocities and their relation to faulting unconstrained. Offshore of Nicaragua, Lefeldt et al. (2012) used a joint tomographic inversion of active-source seismic data and local and regional earthquakes to illuminate the uppermost ~20 km of the mantle. They found that anomalous velocities are related to the depth of normal-fault micro-earthquake activity recorded in the network (Lefeldt et al., 2009), and are considerably shallower than either the rupture depth of large, normal-fault earthquakes or the limit of serpentine stability. Extensional micro-earthquakes indicate that each fault in the region slips every two to three months, which may facilitate regular water percolation. Deeper, large earthquakes are comparatively infrequent, and possibly do not cause significant fracturing that remains open long enough to promote alteration detectable with seismic data. The results show that the stability field of serpentine does not constrain the depth of potential mantle hydration, but suggests that serpentinization is restricted to depth shallower than the neutral plane of plate bending (Lefeldt et al., 2012).

However, at the Cascadia trench, the subducting Juan de Fuca plate does not show any evidence that the mantle has been altered by serpentinization (Table 1; Horning et al., 2016). Consequently, other mechanisms may contribute to governing hydration prior to subduction. Horning et al. (2016) assessed the temperature of the incoming plate and found temperatures at the Moho of ~450 °C, indicating that talc rather than serpentine is probably the primary mode of hydration. Consequently, mantle velocity reduction is very moderate and the amount of bound water trapped in the mantle small. Therefore, bend faulting as an evolutionary process causing serpentinization would be limited to crustal ages of >10–15 Ma, where plate cooling has lowered the mantle temperature to values allowing olivine alteration to serpentine.

CONCLUSIONS

Roughly 10–15 years ago, most scientists considered that the hydration of oceanic plates occurred near mid-ocean ridges and assumed that water would be trapped in the porous upper crust, while the lower crust and upper mantle would remain reasonably dry (e.g., Wallmann, 2001; Jarrard, 2003). However, today scientists have recognized that the process of subduction and bending of the strong and brittle lithosphere at trenches causes normal faulting in the trench-outer rise area, introducing an evolutionary process, altering and hydrating both crustal and upper mantle rocks and hence contributing to volatile fluxes into the Earth interior. Seismic constraints reviewed in this study suggest that serpentinization is a key process to facilitate the flux of water into the mantle. Seismic data support that depending on the thermal state of the incoming plate, subducting lithosphere older than 10–15 Ma carries serpentinized mantle into the trench; serpentinization may range from <4% to up to 20% in the uppermost mantle. Further, the degree of serpentinization of the subducting plate depends on the availability of seawater. Thus, sediment-starved subduction zones may carry larger amounts of chemically bound water into the mantle than subduction zones where the plate is insulated from the ocean by several hundred meters of sediments. However, the style and intensity of bend faulting along trenches are poorly studied. Data from the Nicaraguan trench suggest that future combined P-wave and S-wave studies will be important for studying hydration of the lithosphere prior to subduction.

ACKNOWLEDGMENTS

We thank V. Sallarès and J. Korenaga for their codes to calculate crustal thickness derived from melting models. Digital velocity models were provided by J.P. Canales, E. Contreras-Reyes, A. Dannowski, G. Fujie, R.C. Holmes, E.E.E. Hooft, J.R. Hopper, E. Moscoso, A. Nishizawa, L. Planert, and E. Roland. We are grateful to the German Science Foundation (DFG) for supporting the SFB574 Centre of Excellence. Without the support we would not have been able to conduct the early research in the trench–outer rise. We are very grateful for very helpful comments by the Associate Editor Bob Stern, Jason Phipps Morgan, and two anonymous referees, which improved our manuscript. Figures were produced using the Generic Mapping Tools (GMT) software (Wessel and Smith, 1998).

REFERENCES CITED

Alt, J.C., Honnorez, J., Laverne, C., and Emmerman, R., 1986, Hydrothermal alteration of a 1 km section through the upper oceanic crust, Deep Sea Drilling Project Hole 504B: Mineralogy, chemistry, and evolution of seawater-basalt interactions: Journal of Geophysical Research, v. 91, p. 10,309–10,335, https://doi.org/10.1029/JB091iB10p10309.

Alt, J.C., et al., 1996, Hydrothermal alteration of a section of upper oceanic crust in the eastern equatorial Pacific: A synthesis of results from Site 504 (DSDP Legs 69, 70, and 83, and ODP Legs 111, 137, 140, and 148), *in* Alt, J.C., Kinoshita, H., Stokking, L.B., and Michael, P.J., eds., Proceedings of the Ocean Drilling Program, Scientific Results, Volume 148: College Station, Texas, Ocean Drilling Program, p. 417–434, https://doi.org/10.2973/odp.proc.sr.148.159.1996.

Ammon, C.J., Kanamori, H., and Lay, T., 2008, A great earthquake doublet and seismic stress transfer cycle in the central Kuril islands: Nature, v. 451, p. 561–565, https://doi.org/10.1038/nature06521.

Bodine, J.H., and Watts, A.B., 1979, On lithospheric flexure seaward of the Bonin and Mariana trenches: Earth and Planetary Science Letters, v. 43, p. 132–148, https://doi.org/10.1016/0012-821X(79)90162-6.

Canales, J.P., Detrick, R.S., Bazin, S., Harding, A.J., and Orcutt, J.A., 1998, Off-axis crustal thickness across and along the East Pacific Rise within the MELT area: Science, v. 280, p. 1218–1221, https://doi.org/10.1126/science.280.5367.1218.

Canales, J.P., Detrick, R.S., Lin, J., Collins, J.A., and Toomey, D.R., 2000a, Crustal and upper mantle seismic structure beneath the rift mountains and across a non-transform offset at the Mid-Atlantic Ridge (35°N): Journal of Geophysical Research, v. 105, p. 2699–2719, https://doi.org/10.1029/1999JB900379.

Canales, J.P., Collins, J.A., Escartín, J., and Detrick, R.S., 2000b, Seismic structure across the rift valley of the Mid-Atlantic Ridge at 23°20′ (MARK area): Implications for crustal accretion processes at slow spreading ridges: Journal of Geophysical Research, v. 105, p. 28,411–28,425, https://doi.org/10.1029/2000JB900301.

Canales, J.P., Detrick, R.S., Toomey, D.R., and Wilcock, W.S.D., 2003, Segment-scale variations in the crustal structure of 150–300 kyr old fast spreading oceanic crust (East Pacific Rise, 8°15′N–10°5′N) from wide-angle seismic refraction profiles: Geophysical Journal International, v. 152, p. 766–794, https://doi.org/10.1046/j.1365-246X.2003.01885.x.

Cann, J.R., Blackman, D.K., Smith, D.K., McAllister, E., Janssen, B., Mello, S., Avgerinos, E., Pascoe, A.R., and Escartin, J., 1997, Corrugated slip surfaces formed at ridge-transform intersections on the Mid-Atlantic Ridge: Nature, v. 385, p. 329–332, https://doi.org/10.1038/385329a0.

Carlson, R.L., 1998, Seismic velocities in the uppermost oceanic crust: Age dependence and the fate of layer 2A: Journal of Geophysical Research, v. 103, p. 7069–7077, https://doi.org/10.1029/97JB03577.

Carlson, R.L., and Miller, D.J., 1997, A new assessment of the abundance of serpentinite in the oceanic crust: Geophysical Research Letters, v. 24, p. 457–460, https://doi.org/10.1029/97GL00144.

Carlson, R.L., and Miller, D.J., 2004, Influence of pressure and mineralogy on seismic velocities in oceanic gabbros: Implications for the composition and state of the lower oceanic crust: Journal of Geophysical Research, v. 109, B09205, https://doi.org/10.1029/2003JB002699.

Chapple, W.M., and Forsyth, D.W., 1979, Earthquakes and bending of plates at trenches: Journal of Geophysical Research, v. 84, p. 6729–6749, https://doi.org/10.1029/JB084iB12p06729.

Chen, Y.J., 1992, Oceanic crustal thickness versus spreading rate: Geophysical Research Letters, v. 19, p. 753–756, https://doi.org/10.1029/92GL00161.

Christensen, N.I., 1972, The abundance of serpentinites in the oceanic crust: The Journal of Geology, v. 80, p. 709–719, https://doi.org/10.1086/627796.

Christensen, N.I., 2004, Serpentinites, peridotites, and seismology: International Geology Review, v. 46, p. 795–816, https://doi.org/10.2747/0020-6814.46.9.795.

Contreras-Reyes, E., Grevemeyer, I., Flueh, E.R., Scherwath, M., and Heesemann, M., 2007, Alteration of the subducting oceanic lithosphere at the southern central Chile trench-outer rise: Geochemistry Geophysics Geosystems, v. 8, Q07003, https://doi.org/10.1029/2007GC001632.

Contreras-Reyes, E., Grevemeyer, I., Flueh, E.R., and Reichert, C., 2008, Upper lithospheric structure of the subduction zone offshore of southern Arauco peninsula, Chile, at ~38°S: Journal of Geophysical Research, v. 113, B07303, https://doi.org/10.1029/2007JB005569.

Contreras-Reyes, E., Grevemeyer, I., Watts, A.B., Planert, L., Flueh, E.R., and Peirce, C., 2010, Crustal intrusion beneath the Louisville hotspot track: Earth and Planetary Science Letters, v. 289, p. 323–333, https://doi.org/10.1016/j.epsl.2009.11.020.

Contreras-Reyes, E., Grevemeyer, I., Watts, A.B., Flueh, E.R., Peirce, C., Moeller, S., and Papenberg, C., 2011, Deep seismic structure of the Tonga subduction zone: Implications for mantle hydration, tectonic erosion, and arc magmatism: Journal of Geophysical Research, v. 116, B10103, https://doi.org/10.1029/2011JB008434.

Contreras-Reyes, E., Becerra, J., Kopp, H., Reichert, C., and Díaz-Naveas, J., 2014, Seismic structure of the north-central Chilean convergent margin: Subduction erosion of a paleomagmatic arc: Geophysical Research Letters, v. 41, p. 1523–1529, https://doi.org/10.1002/2013GL058729.

Contreras-Reyes, E., Ruiz, J.A., Becerra, J., Kopp, H., Reichert, C., Maksymowicz, A., and Arriagada, C., 2015, Structure and tectonics of the central Chilean margin (31°–33°S): Implications for subduction erosion and shallow crustal seismicity: Geophysical Journal International, v. 203, p. 776–791, https://doi.org/10.1093/gji/ggv309.

Dalton, C.A., Langmuir, C.H., and Gale, A., 2014, Geophysical and geochemical evidence for deep temperature variations beneath mid-ocean ridges: Science, v. 344, p. 80–83, https://doi.org/10.1126/science.1249466.

Dannowski, A., Grevemeyer, I., Ranero, C.R., Ceuleneer, G., Maia, M., Morgan, J.P., and Gente, P., 2010, Seismic structure of an oceanic core complex at the Mid-Atlantic Ridge, 22°19′N: Journal of Geophysical Research, v. 115, B07106, https://doi.org/10.1029/2009JB006943.

Dannowski, A., Grevemeyer, I., Phipps Morgan, J.P., Ranero, C.R., Maia, M., and Klein, G., 2011, Crustal structure of the propagating TAMMAR ridge segment on the Mid-Atlantic Ridge, 21.5°N: Geochemistry Geophysics Geosystems, v. 12, Q07012, https://doi.org/10.1029/2011GC003534.

Dick, H.J.B., and Zhou, H., 2014, Ocean rises are products of variable mantle composition, temperature and focused melting: Nature Geoscience, v. 8, p. 68–74, https://doi.org/10.1038/ngeo2318.

Emry, E.L., and Wiens, D.A., 2015, Incoming plate faulting in the Northern and Western Pacific and implications for subduction zone water budgets: Earth and Planetary Science Letters, v. 414, p. 176–186, https://doi.org/10.1016/j.epsl.2014.12.042.

Faccenda, M., Gerya, T.V., and Burlini, L., 2009, Deep slab hydration induced by bending-related variations in tectonic pressure: Nature Geoscience, v. 2, p. 790–793, https://doi.org/10.1038/ngeo656.

Freundt, A., Grevemeyer, I., Rabbel, W., Hansteen, T.H., Hensen, C., Wehrmann, H., Kutterolf, S., Halama, R., and Frische, M., 2014, Volatile (H_2O, CO_2, Cl, S) budget of the Central American subduction zone: International Journal of Earth Sciences, v. 103, p. 2101–2127, https://doi.org/10.1007/s00531-014-1001-1.

Fujie, G., Kodaira, S., Yamashita, M., Sato, T., Takahashi, T., and Takahashi, N., 2013, Systematic changes in the incoming plate structure at the Kuril trench: Geophysical Research Letters, v. 40, p. 88–93, https://doi.org/10.1029/2012GL054340.

Gillis, K.M., and Sapp, K., 1997, Distribution of porosity in a section of upper oceanic crust exposed in the Troodos ophiolite: Journal of Geophysical Research, v. 102, p. 10,133–10,149, https://doi.org/10.1029/96JB03909.

Green, H.W., and Houston, H., 1995, The mechanics of deep earthquakes: Annual Review of Earth and Planetary Sciences, v. 23, p. 169–213, https://doi.org/10.1146/annurev.ea.23.050195.001125.

Grevemeyer, I., and Bartetzko, A., 2004, Hydrothermal ageing of oceanic crust: Inferences from seismic refraction and borehole studies, *in* Davis, E.E., and Elderfield, H., eds., Hydrogeology of Oceanic Lithosphere: New York, Cambridge University Press, p. 128– 150.

Grevemeyer, I., and Weigel, W., 1996, Seismic velocities of the uppermost igneous crust versus age: Geophysical Journal International, v. 124, p. 631–635, https://doi.org/10.1111/j.1365-246X.1996.tb07041.x.

Grevemeyer, I., and Weigel, W., 1997, Increase of seismic velocities in upper oceanic crust: The "superfast" spreading East Pacific Rise at 14°14′S: Geophysical Research Letters, v. 24, p. 217–220, https://doi.org/10.1029/96GL04005.

Grevemeyer, I., Weigel, W., and Jennrich, C., 1998, Structure and ageing of oceanic crust at 14°S on the East Pacific Rise: Geophysical Journal International, v. 135, p. 573–584, https://doi.org/10.1046/j.1365-246X.1998.00673.x.

Grevemeyer, I., Flueh, E.R., Reichert, C., Bialas, J., Kläschen, D., and Kopp, C., 2001, Crustal architecture and deep structure of the Ninetyeast Ridge hotspot trail from active-source ocean bottom seismology: Geophysical Journal International, v. 144, p. 414–431, https://doi.org/10.1046/j.0956-540X.2000.01334.x.

Grevemeyer, I., Kaul, N., Diaz-Naveas, J.L., Villinger, H.W., Ranero, C.R., and Reichert, C., 2005, Heat flow and bending-related faulting at subduction trenches: Case studies offshore Nicaragua and central Chile: Earth and Planetary Science Letters, v. 236, p. 238–248, https://doi.org/10.1016/j.epsl.2005.04.048.

Grevemeyer, I., Ranero, C.R., Flueh, E.R., Kläschen, D., and Bialas, J., 2007, Passive and active seismological study of bending-related faulting and mantle serpentinization at the Middle America trench: Earth and Planetary Science Letters, v. 258, p. 528–542, https://doi.org/10.1016/j.epsl.2007.04.013.

Hess, H.H., 1964, Seismic anisotropy of the uppermost mantle under oceans: Nature, v. 203, p. 629–631, https://doi.org/10.1038/203629a0.

Holmes, R.C., Tolstoy, M., Cochran, J.R., and Floyd, J.S., 2008, Crustal thickness variations along the Southeast Indian Ridge (100°-116°E) from 2-D body wave tomography: Geochemistry Geophysics Geosystems, v. 9, Q12020, https://doi.org/10.1029/2008GC002152.

Holmes, R.C., Tolstoy, M., Harding, A.J., Orcutt, J.A., and Morgan, J.P., 2010, Australian Antarctic Discordance as a simple mantle boundary: Geophysical Research Letters, v. 37, L09309, https://doi.org/10.1029/2010GL042621.

Hooft, E.E.E., Detrick, R.S., Toomey, D.R., Collins, J.A., and Lin, J., 2000, Crustal thickness and structure along three contrasting spreading segments of the Mid-Atlantic Ridge, 33.5°–35°N: Journal of Geophysical Research, v. 105, p. 8205–8226, https://doi.org/10.1029/1999JB900442.

Hopper, J.R., Dahl-Jensen, T., Holbrook, W.S., Larsen, H.C., Lizarralde, D., Korenaga, J., Kent, G.M., and Kelemen, P.B., 2003, Structure of the SE Greenland margin from seismic reflection and refraction data: Implications for nascent spreading center subsidence and asymmetric crustal accretion during North Atlantic opening: Journal of Geophysical Research, v. 108, 2269, https://doi.org/10.1029/2002JB001996.

Horning, G., Canales, J.P., Carbotte, S.M., Han, S., Carton, H., Nedimovic, M.R., and van Keken, P.E., 2016, A 2-D tomographic model of the Juan de Fuca plate from accretion at axial seamount to subduction at the Cascadia margin from an active source ocean bottom seismometer survey: Journal of Geophysical Research, v. 121, p. 5859–5879, https://doi.org/10.1002/2016JB013228.

Hunter, J., and Watts, A.B., 2016, Gravity anomalies, flexure and mantle rheology seaward of circum-Pacific trenches: Geophysical Journal International, v. 207, p. 288–316, https://doi.org/10.1093/gji/ggw275.

Hyndman, R.D., and Drury, M.J., 1976, The physical properties of oceanic basement rocks from deep drilling on the Mid-Atlantic Ridge: Journal of Geophysical Research, v. 81, p. 4042–4052, https://doi.org/10.1029/JB081i023p04042.

Ivandic, M., 2008, Impact of bending-related faulting on the seismic properties of the incoming oceanic lithosphere offshore of Nicaragua [Ph.D. thesis]: Kiel, Christian-Albrechts-University, 109 p.

Ivandic, M., Grevemeyer, I., Berhorst, A., Flueh, E.R., and McIntosh, K., 2008, Impact of bending related faulting on the seismic properties of the incoming oceanic plate offshore of Nicaragua: Journal of Geophysical Research, v. 113, B05410, https://doi.org/10.1029/2007JB005291.

Ivandic, M., Grevemeyer, I., Bialas, J., and Petersen, C.J., 2010, Serpentinization in the trench-outer rise region offshore of Nicaragua: Constraints from seismic refraction and wide-angle data: Geophysical Journal International, v. 180, p. 1253–1264, https://doi.org/10.1111/j.1365-246X.2009.04474.x.

Iyer, K., Rüpke, L.H., Morgan, J.P., and Grevemeyer, I., 2012, Controls of faulting and reaction kinetics on serpentinization and double Benioff zones: Geochemistry Geophysics Geosystems, v. 13, Q09010, https://doi.org/10.1029/2012GC004304.

Jackson, H.R., Reid, I., and Falconer, R.K.H., 1982, Crustal structure near the Arctic mid-ocean ridge: Journal of Geophysical Research, v. 87, p. 1773–1783, https://doi.org/10.1029/JB087iB03p01773.

Jarrard, R.D., 2003, Subduction fluxes of water, carbon dioxide, chlorine, and potassium: Geochemistry Geophysics Geosystems, v. 4, 8905, https://doi.org/10.1029/2002GC000392.

Jokat, W., and Schmidt-Aursch, M.C., 2007, Geophysical characteristics of the ultraslow spreading Gakkel Ridge, Arctic Ocean: Geophysical Journal International, v. 168, p. 983–998, https://doi.org/10.1111/j.1365-246X.2006.03278.x.

Karson, J.A., Collins, J.A., and Casey, J.F., 1984, Geologic and seismic velocity structure of the crust/mantle transition in the Bay of Islands ophiolite complex: Journal of Geophysical Research, v. 89, p. 6126–6138, https://doi.org/10.1029/JB089iB07p06126.

Klein, E.M., and Langmuir, C.H., 1987, Global correlations of oceanic ridge basalt chemistry with axial depth and crustal thickness: Journal of Geophysical Research, v. 92, p. 8089–8115, https://doi.org/10.1029/JB092iB08p08089.

Korenaga, J., 2017, On the extent of mantle hydration caused by plate bending: Earth and Planetary Science Letters, v. 457, p. 1–9, https://doi.org/10.1016/j.epsl.2016.10.011.

Korenaga, J., Holbrook, W.S., Kent, G.M., Kelemen, P.B., Detrick, R.S., Larsen, H.-C., Hopper, J.R., and Dahl-Jensen, T., 2000, Crustal structure of the southeast Greenland margin from joint refraction and reflection seismic tomography: Journal of Geophysical Research, v. 105, p. 21,591–21,614, https://doi.org/10.1029/2000JB900188.

Korenaga, J., Kelemen, P.B., and Holbrook, W.S., 2002, Methods for resolving the origin of large igneous provinces from crustal seismology: Journal of Geophysical Research, v. 107, p. 2178, https://doi.org/10.1029/2001JB001030.

Kuo, B.Y., and Forsyth, D.W., 1988, Gravity anomalies of the ridge-transform system in the south Atlantic between 31 and 34.5°S: Upwelling centers and variations in crustal thickness: Marine Geophysical Researches, v. 10, p. 205–232, https://doi.org/10.1007/BF00310065.

Lefeldt, M., and Grevemeyer, I., 2008, Centroid depth and mechanism of trench-outer rise earthquakes: Geophysical Journal International, v. 172, p. 240–251, https://doi.org/10.1111/j.1365-246X.2007.03616.x.

Lefeldt, M., Grevemeyer, I., Goßler, J., and Bialas, J., 2009, Intraplate seismicity and related mantle hydration at the Nicaraguan trench outer rise: Geophysical Journal International, v. 178, p. 742–752, https://doi.org/10.1111/j.1365-246X.2009.04167.x.

Lefeldt, M., Ranero, C.R., and Grevemeyer, I., 2012, Seismic evidence of tectonic control on the depth of water influx into incoming oceanic plates at subduction trenches: Geochemistry Geophysics Geosystems, v. 13, Q05013, https://doi.org/10.1029/2012GC004043.

Levitt, D.A., and Sandwell, D.T., 1995, Lithospheric bending at subduction zones based on depth soundings and satellite gravity: Journal of Geophysical Research, v. 100, p. 379–400, https://doi.org/10.1029/94JB02468.

Li, J., et al., 2015, Seismic observation of an extremely magmatic accretion at the ultraslow spreading Southwest Indian Ridge: Geophysical Research Letters, v. 42, p. 2656–2663, https://doi.org/10.1002/2014GL062521.

Lin, J., and Phipps Morgan, J., 1992, The spreading rate dependence of three-dimensional mid-ocean ridge gravity structure: Geophysical Research Letters, v. 19, p. 13–16, https://doi.org/10.1029/91GL03041.

Martin, B., and Fyfe, W.S., 1970, Some experimental and theoretical observations on the kinetics of hydration reactions with particular reference to serpentinization: Chemical Geology, v. 6, p. 185–202, https://doi.org/10.1016/0009-2541(70)90018-5.

Masson, D.G., 1991, Fault patterns at outer trench walls: Marine Geophysical Researches, v. 13, p. 209–225, https://doi.org/10.1007/BF00369150.

McKenzie, D., and Bickle, M.J., 1988, The volume and composition of melt generated by extension of the lithosphere: Journal of Petrology, v. 29, p. 625–679, https://doi.org/10.1093/petrology/29.3.625.

Miller, C.M., and Lizarralde, D., 2016, Finite-frequency wave propagation through outer rise fault zones and seismic measurements of upper mantle hydration: Geophysical Research Letters, v. 43, p. 7982–7990, https://doi.org/10.1002/2016GL070083.

Minshull, T.A., White, R.S., Mutter, J.C., Buhl, P., Detrick, R.S., Williams, C.A., and Morris, E., 1991, Crustal structure at the Blake Spur Fracture Zone from expanding spread profiles: Journal of Geophysical Research, v. 96, p. 9955–9984, https://doi.org/10.1029/91JB00431.

Minshull, T.A., Muller, M.R., and White, R.S., 2006, Crustal structure of the Southwest Indian Ridge at 66°E: Seismic constraints: Geophysical Journal International, v. 166, p. 135–147, https://doi.org/10.1111/j.1365-246X.2006.03001.x.

Moscoso, E., and Grevemeyer, I., 2015, Bending-related faulting of the incoming oceanic plate and its effect on lithospheric hydration and seismicity: A passive and active seismological study offshore Maule, Chile: Journal of Geodynamics, v. 90, p. 58–70, https://doi.org/10.1016/j.jog.2015.06.007.

Moscoso, E., Grevemeyer, I., Contreras-Reyes, E., and Flueh, E.R., 2011, Revealing the deep structure and rupture plane of the 2010 Maule, Chile earthquake (Mw = 8.8) using wide angle seismic data: Earth and Planetary Science Letters, v. 307, p. 147–155, https://doi.org/10.1016/j.epsl.2011.04.025.

Naif, S., Key, K., Constable, S., and Evans, R.L., 2015, Water-rich bending faults at the Middle America Trench: Geochemistry Geophysics Geosystems, v. 16, p. 2582–2597, https://doi.org/10.1002/2015GC005927.

Niu, X., Ruan, A., Li, J., Minshull, T.A., Sauter, D., Wu, Z., Qiu, X., Zhao, M., Chen, Y.J., and Singh, S., 2015, Along axis variation in crustal thickness at the ultraslow spreading Southwest Indian Ridge (50°) from a wide-angle seismic experiment: Geochemistry Geophysics Geosystems, v. 16, p. 468–485, https://doi.org/10.1002/2014GC005645.

Oikawa, M., Kaneda, K., and Nishizawa, A., 2010, Seismic structures of the 154–160 Ma oceanic crust and uppermost mantle in the Northwest Pacific Basin: Earth, Planets, and Space, v. 62, p. e13–e16, https://doi.org/10.5047/eps.2010.02.011.

Peacock, S.M., 2004, Insight into the hydrogeology and alteration of oceanic lithosphere based on subduction zones and arc volcanism, *in* Davis, E.E., and Elderfield, H., eds., Hydrogeology of Oceanic Lithosphere: New York, Cambridge University Press, p. 659–676.

Perfit, M.R., and Chadwick, W.W., 1998, Magmatism at mid-ocean ridges: Constraints from volcanological and geochemical investigations, *in* Buck, W.R., Delaney, P.T., Karson, J.A., and Lagabrielle, Y., eds., Faulting and Magmatism at Mid-Ocean Ridges: American Geophysical Union Geophysical Monograph 106, p. 59–115, https://doi.org/10.1029/GM106p0059.

Planert, L., Flueh, E.R., and Reston, T.J., 2009, Along- and across-axis variations in crustal thickness and structure at the Mid-Atlantic Ridge at 5°S obtained from wide-angle seismic tomography: Implications for ridge segmentation: Journal of Geophysical Research, v. 114, B09102, https://doi.org/10.1029/2008JB006103.

Planert, L., Kopp, H., Lueschen, E., Mueller, C., Flueh, E.R., Shulgin, A., Djajadihardja, Y., and Krabbenhoeft, A., 2010, Lower plate structure and upper plate deformational segmentation at the Sunda-Banda arc transition, Indonesia: Journal of Geophysical Research, v. 115, B08107, https://doi.org/10.1029/2009JB006713.

Popp, T., and Kern, H., 1994, The influence of dry and water saturated cracks on seismic velocities of crustal rocks—A comparison of experimental data with theoretical models: Surveys in Geophysics, v. 15, p. 443–465, https://doi.org/10.1007/BF00690169.

Purdy, G.M., and Detrick, R.S., 1986, Crustal structure of the Mid-Atlantic Ridge at 23°N from seismic refraction studies: Journal of Geophysical Research, v. 91, p. 3739–3762, https://doi.org/10.1029/JB091iB03p03739.

Raitt, R.W., 1963, The crustal rocks, *in* Hill, M.N., ed., The Sea, Vol. 3: The Earth Beneath the Sea History: New York, Interscience, p. 85–102.

Ranero, C.R., and Sallarès, V., 2004, Geophysical evidence for hydration of the crust and mantle of the Nazca plate during bending at the north Chile Trench: Geology, v. 32, p. 549–552, https://doi.org/10.1130/G20379.1.

Ranero, C.R., Morgan, J.P., McIntosh, K., and Reichert, C., 2003, Bending-related faulting and mantle serpentinization at the Middle America Trench: Nature, v. 425, p. 367–373, https://doi.org/10.1038/nature01961.

Ranero, C.R., Villaseñor, A., Morgan, J.P., and Weinrebe, W., 2005, Relationship between bend-faulting at trenches and intermediate-depth seismicity: Geochemistry Geophysics Geosystems, v. 6, Q12002, https://doi.org/10.1029/2005GC000997.

Reston, T.J., and Ranero, C.R., 2011, The 3-D geometry of detachment faulting at mid-ocean ridges: Geochemistry Geophysics Geosystems, v. 12, Q0AG05, https://doi.org/10.1029/2011GC003666.

Reston, T.J., Ranero, C.R., and Belykh, I., 1999, The structure of Cretaceous oceanic crust of the NW Pacific: Constraints on processes at fast spreading centers: Journal of Geophysical Research, v. 104, p. 629–644, https://doi.org/10.1029/98JB02640.

Roland, E., Lizarralde, D., McGuire, J.J., and Collins, J.A., 2012, Seismic velocity constraints on the material properties that control earthquake behavior at the Quebrada-Discovery-Gofar transform faults, East Pacific Rise: Journal of Geophysical Research, v. 117, B11102, https://doi.org/10.1029/2012JB009422.

Rüpke, L., Phipps Morgan, J., and Dixon, J.E., 2009, Implications of subduction rehydration for Earth's deep water cycle, *in* Jacobsen, S.D., and Van Der Lee, S., eds., Earth's Deep Water Cycle: American Geophysical Union Geophysical Monograph 168, p. 263–276, https://doi.org/10.1029/168GM20.

Rüpke, L.H., Phipps Morgan, J., Hort, M., and Connolly, J.A.D., 2004, Serpentine and the subduction zone water cycle: Earth and Planetary Science Letters, v. 223, p. 17–34, https://doi.org/10.1016/j.epsl.2004.04.018.

Sallarès, V., Charvis, P., Flueh, E.R., and Bialas, J., and the SALIERI Scientific Party, 2005, Seismic structure of the Carnegie ridge and the nature of the Galápagos hotspot: Geophysical Journal International, v. 161, p. 763–788, https://doi.org/10.1111/j.1365-246X.2005.02592.x.

Shillington, D.J., Bécel, A., Nedimovic, M.R., Kuehn, H., Webb, S.C., Abers, G.A., Keranen, K.M., Li, J., Delescluse, M., and Mattei-Salicrup, G.A., 2015, Link between plate fabric, hydration and subduction zone seismicity in Alaska: Nature Geoscience, v. 8, p. 961–964, https://doi.org/10.1038/ngeo2586.

Stein, C.A., and Stein, S., 1994, Constraints on hydrothermal heat flux trough the oceanic lithosphere from global heat flow: Journal of Geophysical Research, v. 99, p. 3081–3095, https://doi.org/10.1029/93JB02222.

Tolstoy, M., Harding, A.J., and Orcutt, J.A., 1993, Crustal thickness on the Mid-Atlantic Ridge: Bull's-eye gravity anomalies and focused accretion: Science, v. 262, p. 726–729, https://doi.org/10.1126/science.262.5134.726.

van Avendonk, H.J.A., Harding, A.J., Orcutt, J.A., and McClain, J.S., 1998, A two-dimensional tomography study of the Clipperton transform fault: Journal of Geophysical Research, v. 103, p. 17,885–17,899, https://doi.org/10.1029/98JB00904.

van Avendonk, H.J.A., Holbrook, W.S., Lizarralde, D., and Denyer, P., 2011, Structure and serpentinization of the subducting Cocos plate offshore Nicaragua and Costa Rica: Geochemistry Geophysics Geosystems, v. 12, Q06009, https://doi.org/10.1029/2011GC003592.

van Avendonk, H.J.A., Davis, J.K., Harding, J.L., and Lawver, L.A., 2017, Decrease in oceanic crustal thickness since the breakup of Pangaea: Nature Geoscience, v. 10, p. 58–61, https://doi.org/10.1038/ngeo2849.

van Keken, P.E., Hacker, B.R., Syracuse, E.M., and Abers, G.A., 2011, Subduction factory: 4. Depth-dependent flux of H_2O from subducting slabs worldwide: Journal of Geophysical Research, v. 116, B01401, https://doi.org/10.1029/2010JB007922.

Wallmann, K., 2001, The geological water cycle and the evolution of marine $\delta^{18}O$ values: Geochimica et Cosmochimica Acta, v. 65, p. 2469–2485, https://doi.org/10.1016/S0016-7037(01)00603-2.

Wang, X.-Q., Schubnel, A., Fortin, J., David, E.C., Guéguen, Y., and Ge, H.-K., 2012, High Vp/Vs ratio: Saturated cracks or anisotropy effects?: Geophysical Research Letters, v. 39, L11307, https://doi.org/10.1029/2012GL051742.

Wessel, P., and Smith, W.H.F., 1998, New, improved version of Generic Mapping Tools released: Eos (Transactions, American Geophysical Union), v. 79, p. 579, https://doi.org/10.1029/98EO00426.

White, R.S., McKenzie, D., and O'Nions, R.K., 1992, Oceanic crustal thickness from seismic measurements and rare earth element inversions: Journal of Geophysical Research, v. 97, p. 19,683–19,715, https://doi.org/10.1029/92JB01749.

White, R.S., Minshull, T.A., Bickle, M., and Robinson, C.J., 2001, Melt generation at very slow-spreading oceanic ridges: Constraints from geochemical and geophysical data: Journal of Petrology, v. 42, p. 1171–1196, https://doi.org/10.1093/petrology/42.6.1171.

White, R.S., Smith, L.K., Roberts, A.W., Christie, F., Kusznir, N.J., and the iSIMM Team, 2008, Lower-crustal intrusion on the North Atlantic continental margin: Nature, v. 452, p. 460–464, https://doi.org/10.1038/nature06687.

Whitmarsh, R.B., 1978, Seismic refraction studies of the upper igneous crust in the North Atlantic and porosity estimates for layer 2: Earth and Planetary Science Letters, v. 37, p. 451–464, https://doi.org/10.1016/0012-821X(78)90061-4.

Wilson, D.S., et al., 2006, Drilling to gabbro in intact ocean crust: Science, v. 312, p. 1016–1020, https://doi.org/10.1126/science.1126090.

Zelt, C.A., and Smith, R.B., 1992, Seismic traveltime inversion for 2-D crustal velocity structure: Geophysical Journal International, v. 108, p. 16–34, https://doi.org/10.1111/j.1365-246X.1992.tb00836.x.